Title: A novel genetic fluorescent reporter to visualize mitochondrial nucleoids

Authors: Jingti Deng[1*], Lucy Swift[2*], Mashiat Zaman[3], Fatemeh Shahhosseini[1], Abhishek Sharma[3] Daniela Bureik[4], Francesco Padovani[4], Alissa Benedikt[4], Amit Jaiswal[3], Craig Brideau[2], Savraj Grewal[3], Kurt M. Schmoller[4], Pina Colarusso[5#], Timothy E. Shutt[6#]

Affiliations:

[1]Department of Medical Genetics, Cumming School of Medicine, University of Calgary, AB.

[2]Live Cell Imaging Laboratory, Snyder Institute for Chronic Diseases, Cumming School of Medicine, University of Calgary, Calgary, AB.

[3]Department of Biochemistry & Molecular Biology, Cumming School of Medicine, University of Calgary, AB.

[4]Institute of Functional Epigenetics, Molecular Targets and Therapeutics Center, Helmholtz Zentrum München, Neuherberg, Germany

[5]Department of Physiology and Pharmacology; Live Cell Imaging Laboratory, Snyder Institute for Chronic Diseases, Cumming School of Medicine, University of Calgary, Calgary, AB.

[6]Departments of Medical Genetics and Biochemistry & Molecular Biology; Snyder Institute for Chronic Diseases; Alberta Children's Hospital Research Institute; Hotchkiss Brain Institute; Cumming School of Medicine, University of Calgary, AB.

[*]Denotes co-first author

[#]Denotes co-corresponding author

Abstract:

Mitochondria have their own genome (mtDNA), which is present in hundreds of copies per cell and organized into nucleoid structures that are distributed throughout the dynamic mitochondrial network. Beyond encoding essential protein subunits for oxidative phosphorylation, mtDNA can also serve as a signalling molecule when it is present into the cytosol. Despite the importance of this genome, there are still many unknowns with respect to its regulation. To study mtDNA dynamics in living cells, we have developed a genetic fluorescent reporter, mt-HI-NESS, which is based on the HI-NESS reporter that uses the bacterial H-NS DNA binding domain. Here, we describe how this reporter can be used to image mtDNA nucleoids for live cell imaging without affecting the replication or expression of the mtDNA. In addition to demonstrating the adaptability of the mt-HI-NESS reporter for multiple fluorescent proteins, we also emphasize important factors to consider during the optimization and application of this reporter.

Introduction

Mitochondria are endosymbiotic organelles that harbour their own genome (mtDNA), evidence of their bacterial origins. In humans, mtDNA is ~16.5 kbp and is located in the mitochondrial matrix; it encodes 2 ribosomal RNAs, 22 tRNAs, and 13 proteins that are essential components of oxidative phosphorylation complexes [1]. Unlike the nuclear genome, mtDNA is circular and is present in hundreds of copies per cell. Although the mtDNA copy number varies in different cell types, the mechanisms regulating this variability are not fully understood. The packaging, maintenance, and expression of mtDNA is carried out by a dedicated set of proteins that are encoded in the nucleus, translated in the cytosol, and imported into mitochondria. The mtDNA is packaged into nucleoid structures, in large part by the mtDNA binding protein TFAM [2], which also acts as a transcription factor in animals [3].

In mammals, nucleoids typically contain ~1.4 mtDNA molecules [4] and are distributed evenly throughout the dynamic mitochondrial network. Impairments in mitochondrial fission and fusion can impact both mtDNA copy number, and the distribution of nucleoids [5–8]. Fission events are implicated in licensing mtDNA replication [9,10], while fusion is thought to be important for an even distribution of the machinery required for mtDNA replication and maintenance [11]. Meanwhile, impairments to either fission [12–15] or fusion [11,16,17] can also lead to clustering of nucleoids into larger aggregates. Further, reductions in mitochondrial fusion can also lead to individual mitochondrial that lack nucleoids entirely [18]. More recently, it is recognized that mtDNA can be released into the cytosol, where it can act as a signaling molecule that triggers innate immune inflammatory pathways [19]. In addition, mtDNA can also be released into extracellular vesicles[20]. However, the exact mechanism mediating cytosolic and extracellular mtDNA release are not fully understood, in part due to technical challenges to visualize mtDNA with microscopy.

The direct visualization of mtDNA distribution and dynamics in living cells is essential for decoding their function. Several tools are available to image mtDNA nucleoids, including immunofluorescence, DNA dyes, and fluorescent protein tags [21]. However, these tools are limited in their applicability for live-cell imaging. For example, immunofluorescence, against either DNA or nucleoid proteins requires fixation, and can thus only provide a snapshot of

mtDNA dynamics. Meanwhile, DNA-specific dyes, such as PicoGreen [22,23] or SYBR Gold [24,25] can label mtDNA for live cell imaging. However, these dyes are not specific for mtDNA as they will bind any DNA in the cell, and can sometimes bind RNA. Moreover, due to their DNA intercalating activity, these dyes can impair mtDNA replication and transcription [21]. Finally, the binding affinity of these dyes can be impacted by the degree of mtDNA packaging, which may prevent intercalation [26]. On the other hand, when considering genetic constructs to label nucleoids, selectivity is a barrier for using fluorescently tagged proteins. Although several nucleoid proteins have been identified, they are not all exclusive to nucleoids (*e.g.*, ATAD3A [26]) or do not label all nucleoids (*e.g.*, TFAM [27], TWINKLE [28], mtSSB [28]). Moreover, overexpression of nucleoid proteins can impact mtDNA regulation (*e.g.*, TFAM [29,30], TWINKLE [31,32], M19 [33]). Thus, using dyes or overexpressing nucleoid proteins tagged with a fluorescent protein can have adverse effects on mtDNA that preclude observing nucleoids in their natural state.

To avoid nucleoid protein overexpression artifacts, it may be possible to introduce a fluorescent protein tag into a particular gene via CRISPR technology, enabling endogenous expression of the tagged nucleoid protein. However, this complex approach is limited in its applicability. It is also possible that adding a tag could impact the function of the tagged nucleoid protein. For example, many fluorescent proteins tend to oligomerize [34], which is known to introduce artefacts [35]. Meanwhile, tagging TFAM, the most well-characterized nucleoid protein may be problematic, as it is targeted to mitochondria via an N-terminal mitochondrial targeting sequence (MTS), as are many proteins that localize to the mitochondrial matrix. Finally, TFAM also has a critical C-terminal region required for its transcription-stimulating activity [36]. Thus, better tools are required to study mtDNA dynamics.

With the goal of developing a non-invasive genetic fluorescent marker to visualize mtDNA nucleoids for live-cell imaging, we have adapted the recently described HI-NESS genetic reporter [37], which fuses a fluorescent protein to the bacterial H-NS DNA binding domain, and labels nuclear DNA without any reported adverse effects [38]. Notably, H-NS-like proteins have a preference for AT-rich sequences [39,40], which should make them ideal for the AT-rich human mtDNA. Despite the bacterial history of mitochondria, the core machinery for their transcription and replication does not resemble typical bacterial machinery, but instead is

derived from T-odd phages [41], and has acquired additional unique regulatory factors [42–44]. Therefore, a HI-NESS reporter is not expected to impact mitochondrial DNA replication or transcription by interacting with this mitochondrial machinery. Thus, as a novel approach to monitor mtDNA nucleoid dynamics, we designed and tested several modified versions of the HI-NESS reporter targeted to mitochondria.

Results

Construct Design – mt-TagRFP-HI-NESS

As with the original HI-NESS construct [37], we started with the DNA binding domain of the *E. coli* H-NS protein (amino acids 80-137; GenBank: EIS4692233.1), which we fused to the C-terminus of a fluorescent protein. We chose to start with the TagRFP fluorescent protein derived *from Entacmaea quadricolor* [45] (GenBank: ABR08320.1), which is established to function in the environment of the mitochondrial matrix [46]. To facilitate immunodetection of the reporter, we added an HA epitope tag (YPYDVPDYA) to the C-terminus of the H-NS DNA binding domain, which has previously been shown not to interfere with DNA binding of the H-NS protein [47]. Next, a double Cox8 MTS [48], shown to improve the mitochondrial import of fluorescent proteins [49], was added to the N-terminus of the construct to target the reporter to mitochondria. The MTS is followed by an unstructured linker sequence (GDPPVAT) used previously for fluorescent proteins localized to the mitochondrial matrix [50].

The organization of this initial open reading frame, which we refer to as mt-TagRFP-HI-NESS, is shown in Figure 1, along with a predicted 3D model generated using AlphaFold 2 [51]. The nucleotide and protein sequences for this reporter can be found in the supplemental material (Fig S1). While the full-length protein is predicted at 40.6 kDA, the MTS is often cleaved and processed by a series of mitochondrial proteases [52]. Using existing programs available to predict the MTS cleavage site, the mt-TagRFP-HI-NESS protein is predicted to be cleaved either after residue L43 (MitoFates [53]) or K56 (TargetP2.0 [54]), resulting a mature protein predicted of 34.7 kDa or 36 kDa, respectively.

VectorBuilder (Chicago, IL, USA) was commissioned to synthesize the mt-HI-NESS-TagRFP open reading frame and insert it into a lentiviral mammalian gene expression vector. The lentivirus vector expresses the mt-TagRFP-HI-NESS open reading frame under an hPGK promoter and contains puromycin and ampicillin selection markers. The vector ID for mt-TagRFP-HI-NESS is VB221222-1228fqm, which can be used to retrieve detailed information about the vector of vectorbuilder.com. A vector map (Fig S2) and the DNA sequence (Fig S3) are provided in the supplemental material.

Characterization of mt-TagRFP-HI-NESS

We generated lentivirus that was used to transduce U2OS cells for stable expression of mt-Tag-RFP-HI-NESS. Flow cytometry was used to select cells expressing TagRFP, and these cells were imaged using live-cell confocal microscopy. Notably, the expression level of TagRFP was variable among different cells (Fig 2A). Nonetheless, we consistently observed TagRFP signal localizing to punctate spots that were confirmed to be nucleoids through co-staining with SYBR gold to label mtDNA (Fig 2B), or MitoTracker Green to label the mitochondrial network (Fig 2C). While this initial imaging suggested proof of principle that mt-TagRFP-HI-NESS could be used for live cell imaging of nucleoids, we also noted that in a significant number of cells there was non-nucleoid specific TagRFP signal that was distributed throughout the mitochondrial network. Notably, through single-cell cloning, we were able to isolate cell lines with mitochondrial nucleoid-specific TagRFP signal that lacked any non-specific mitochondrial network signal (Fig 3A,B). To test if the non-nucleoid mitochondrial TagRFP signal was due to excess mt-Tag-RFP-HI-NESS protein expression, essentially swamping out the available DNA binding sites, we used flow cytometry to sort cells based on levels of TagRFP expression into four bins: low, medium-low, medium-high, and high (Fig 4A & S4A). Confocal imaging across all expression levels again showed some cells with underlying TagRFP signal that is not specific for nucleoids though it was specific for the mitochondrial network (Fig S4B), suggesting this non-nucleoid localization was not an overexpression artefact.

Next, we tested if mt-TagRFP-HI-NESS expression impacted mtDNA maintenance and expression. To this end, we took advantage of our cell populations sorted by TagRFP expression.

Western blotting with anti-HA confirmed the variable protein expression in our cell populations, and revealed no changes in the expression of VDAC1 or HSP60 mitochondrial proteins often used to measure mitochondrial abundance (Fig 4A). In addition, the expression of protein subunits for all five oxidative phosphorylation complexes (CI-CV), including mtDNA-encoded MTCOI, was unaltered. When we proceeded to look at mtDNA copy number by quantitative PCR we saw no significant differences in most lines (Fig 4B). However, there was a significant reduction (~30%) in mtDNA copy number in cells expressing the highest levels of mt-TagRFP-HI-NESS, which suggests caution is warranted when the reporter is highly expressed. Finally, we examined steady-state levels of mtDNA-encoded transcripts via q-RT-PCR (Fig 4C). While we did not see any significant differences in transcript levels, it is notable that the results were variable, which may reflect a technical issue with this approach.

Double HI-NESS

Given that sorting by TagRFP expression level did not mitigate the non-specific mitochondrial labelling in some cells, we reasoned that the mt-TagRFP-HI-NESS protein may not be binding to mtDNA efficiently. Thus, we set out to modify our original construct by adding a second H-NS DNA binding domain to increase binding efficiency. We considered two possibilities (Fig 5A,B). The first option was adding a second H-NS domain immediately after the K56 cleavage site in the MTS, such that one H-NS domain was at the N-terminus and the second was at the C-terminus (N/C). The second option was to add a second H-NS domain at the C-terminus, immediately after the HA tag, such that both H-NS domains were at the C-terminus (C/C). Ultimately, we decided to test the N/C double HI-NESS construct. To avoid repetitive sequences in the open reading frame that might have adverse effects on plasmid and/or viral propagation, we took advantage of the degeneracy in codon usage to change the nucleotide sequence without changing the encoded protein domain. To this end, the codon sequence for the N-terminal H-NS domain was 'humanized' by choosing codons more commonly used in the human genome. This modified reporter, mt-TagRFP-N/C-HI-NESS, has a predicted full-length size of 47 kDa, and a predicted processed size of 43.3 kDa (MitoFates) or 41 kDa (TargetP 2.0). The vector ID for mt-TagRFP-N/C-HI-NESS is VB230529-1292kdj, which can be used to retrieve

detailed information about the vector of vectorbuilder.com. A vector map and the DNA sequence is provided in the supplemental material (Fig S2&3). When we tested the mt-TagRFP-N/C-HI-NESS reporter expressed in U2OS following stable viral transduction, we observed a significant improvement in nucleoid-specific staining, with much less non-specific mitochondrial localization (Fig 5C,D).

Mt-Kaede-HI-NESS

Given the initial success of the mt-TagRFP-HI-NESS reporter in labelling mtDNA nucleoids, we wanted to take advantage of the palette of available fluorescent proteins available for live-cell imaging, including photoconvertible properties that can be taken advantage of to better understand biological processes. To this end, we started with Kaede, a photoconvertible fluorescent protein derived from *Trachyphyllia geoffroyi*, which when activated by UV or violet light, permanently switches its fluorescence emission from red to green [55]. By replacing the TagRFP domain with Kaede, in our original mt-TagRFP-HI-NESS construct, we generated a mt-Kaede-HI-NESS reporter with a predicted full-length size of 40.2 kDa, and a predicted processed size of 35.6 kDa (MitoFates) or 34.2 kDa (TargetP 2.0) (Fig 6A,B). The vector ID for mt-Kaede-HI-NESS is VB230322-1526htn, which can be used to retrieve detailed information about the vector of vectorbuilder.com. A vector map and the DNA sequence is provided in the supplemental material (Fig S2&3).

Initial imaging with U2OS cells stably transduced to express mt-Kaede-HI-NESS revealed specific punctate signal within the mitochondrial network, as imaged with MitoTracker Deep Red (Fig 6C). Remarkably, we observed only puncta with the mt-Kaede-HI-NESS reporter, without any of the mitochondrial network labelling sometimes seen with the original mt-mTagRFP-HI-NESS reporter. This observation suggests that the TagRFP protein properties hinder the DNA binding capacity of the H-NS domain. Highlighting the utility of the mt-Kaede-HI-NESS reporter, we were able to successfully photoconvert a subset of nucleoids and follow these nucleoids over time with live cell imaging (Fig 6D).

Applications

Given the superior nucleoid labelling of the mt-Kaede-HI-NESS reporter, we focused on this reporter. While viral transduction provides stable cell lines that can be repeatedly studied, selection can be tedious and time-consuming. Thus, we compared mtDNA nucleoids in our stably transduced lentiviral mt-Kaede-HI-NESS cells with U2OS cells transiently transfected with the mt-Kaede-HI-NESS reporter (Fig 7A). While there are some differences in the distribution of mtDNA nucleoid sizes and numbers between stable and transient mt-Kaede-HI-NESS expression (Fig 7B,C), it is unclear whether the larger distribution of sizes is due to different expression levels or the stress of the transfection. We next wanted to test the ability of the mt-Kaede-HI-NESS reporter to visualize changes in mitochondrial nucleoids and to track dynamic events such as cytosolic and extracellular mtDNA release.

Nucleoid dynamics

To examine if the mt-Kaede-HI-NESS reporter can be used to see changes in nucleoid dynamics, we used U2OS MFN2$^{-/-}$ cells [56], as loss of the mitochondrial fusion protein MFN2 leads to fragmented mitochondrial networks and altered mtDNA characteristics and distribution [11,57]. As expected, following transient transfection of mt-Kaede-HI-NESS into U2OS control or U2OS MFN2$^{-/-}$, cells lacking MFN2 had nucleoids that were larger and fewer in number compared to control, as well as a subset of mitochondria lacking nucleoids and (Fig 7).

Cytosolic mtDNA release

We then looked to see if the mt-Kaede-HI-NESS reporter could be used to visualize mtDNA that had escaped into the cytosol. We first used two established genetic models of mtDNA release, MFN2$^{-/-}$ [58] and TFAM$^{-/+}$ [59,60], as we were able to obtain both genotypes in U2OS cells. In both cases, following transient transfection, we were able to visualize and quantify cytosolic mtDNA using the mt-Kaede-HI-NESS reporter (Fig 8A,B). Next, we treated our stably transduced mt-Kaede-HI-NESS cells with LPS (20ug/ml for 12 hours) or dexamethasone (200nM for 18 hours), two treatments that induce cytosolic mtDNA release [61,62]. Again, both treatments lead to an increase in cytosolic mtDNA puncta (Fig 8C-G). Notably, while LPS treatment led to fewer nucleoids and fragmented mitochondrial networks, dexamethasone had no effect on

copy number, but increased elongation of the mitochondrial network. Together these finding show that the mt-Kaede-HI-NESS reporter can be used to image cytosolic mtDNA release under a variety of conditions.

Extracellular mtDNA release

To examine the release of mtDNA into extracellular vesicles (EVs) we used our stably transduced mt-Kaede-HI-NESS cells and looked both basally and following overnight treatment with LPS (2 µg/ml) in FBS-free medium to stimulate the formation of EVs [63] (Fig 9). Following immunocapture of EVs with a CD13 antibody [63] (Fig 9A,B), we were also able to visualize the mt-Kaede-HI-NESS protein by confocal imaging in a subset of EVs, and quantify that LPS treatment increased the size of EVs, and the percentage of Kaede positive EVs (Fig 9C-H). Additionally, Immunoblotting of the cellular and extracellular material following differential centrifugation showed the presence of the mt-Kaede-HI-NESS protein (probed with anti-HA) in the extracellular fraction, which was enriched upon LPS treatment (Fig 9J). Finally, quantitative PCR also confirmed the presence of mtDNA in the extracellular fraction and enrichment upon LPS treatment (Fig 9I). Collectively, this work demonstrates that the mt-Kaede-HI-NESS reporter can be used to monitor the release of mtDNA via EVs.

Nucleoid labelling in other systems

We also wanted to test the ability of the mt-Kaede-HI-NESS reporter to label mtDNA in other biological systems. While another report highlights the utility of mt-Kaede-HI-NESS reporter in plants (*Arabidopsis thaliana*) [64], here we also show its applicability in both yeast (*Saccharomyces cerevisiae*) and fruit fly (*Drosophila melanogaster*).

S. cerevisiae

To test whether the mt-Kaede-HI-NESS reporter can be adapted to visualize mtDNA in budding yeast, we constructed strains in which we integrated mt-Kaede-HI-NESS into the *URA3* locus, N-terminally tagged with a Su9 mitochondrial targeting sequence, and expressed from four different promoters chosen to cover a broad range of expression strengths [65] (Fig.10A). In

addition, each strain expressed Su9-mKate2 as a fluorescent reporter for the mitochondrial network [66]. With qPCR, we found that when expressed from the *RPL25* promoter, i.e. the strongest promoter tested, the mt-Kaede-HI-NESS reporter leads to a significantly reduced mtDNA copy number per cell during exponential growth on SCD medium (synthetic complete medium with 2% glucose as carbon source) (Fig. 10B). By contrast, cells expressing the reporter from the *MLC1*, *CUP1*, or *ACT1* promoters have similar mtDNA copy numbers (Fig. 10B), cell volumes (Fig. S6A) and bud fractions (Fig. S6B) compared to wild-type cells, and do not show any obvious growth defects. We also verified that the strains grow on respiratory media with 2% glycerol and 1% ethanol as carbon sources, in which functional mtDNA is essential.

With live-cell confocal microscopy, we then found that when the reporter was expressed from the *MLC1* promoter, although clearly localized to the mitochondrial network, the signal was very weak and barely above the background (Fig. S6C-D). However, when expressed from the *CUP1* or *ACT1* promoters, we observed clear spot-like signal located in the mitochondrial network, as expected for mtDNA containing nucleoids (Fig. 10D, Fig. S6C-D). In the case of the *ACT1* promoter, the signal was cleaner compared to the *CUP1* promoter (Fig. S6C-D), and required lower excitation intensities (Fig. 10D). For all promoters, the mitochondrial network volume is very similar to the control strain without mt-Kaede-HI-NESS reporter (Fig. S6E). Next, we used SpotMAX [67] for automated spot counting, and found that cells contained about 8 resolvable spots in the case of the *ACT1* promoter, which is consistent with what is expected based on similar experiments performed using a LacO-LacI based reporter system, the current gold-standard for mtDNA live-cell imaging in budding yeast [66,68] (Fig. 10C,D). In the case of the *CUP1* promoter, we only detected about 5 clear spots per cell, likely due to the lower signal-to-noise ratio. To further verify that the observed spots correspond to mt-Kaede-HI-NESS bound to mtDNA, we made use of the fact that mtDNA is not essential for budding yeast growth on fermentable media. We deleted the mitochondrial DNA polymerase *MIP1*, resulting in the loss of mtDNA (Fig. S6F). Indeed, in *mip1Δ* cells, the mt-Kaede-HI-NESS signal is delocalized throughout the mitochondrial network and does not localize in spots (Fig. 10C,D). Taken together, mt-Kaede-HI-NESS can be used as a fluorescent reporter for mtDNA in live budding yeast cells. Expression from the strong *ACT1* promoter provides a high signal-to-

noise ratio even at lower excitation intensities well suited for live-cell imaging, without any obvious perturbations of mtDNA and cell function.

D. melanogaster

To test the mt-Kaede-HI-NESS reporter in an animal model, we took advantage of *Drosophila* melanogaster and the UAS expression system. We first generated a line carrying the mt-Kaede-HI-NESS open reading frame under control the UAS promoter/enhancer. The UAS-mt-Kaede-HI-NESS reporter transgenic line was crossed to the daughterless-Gal4 line to drive ubiquitous expression of the UAS-mt-Kaede-HI-NESS. Following the isolation of fat body from larvae, we were able to image mt-Kaede-HI-NESS signal, which localized within the mitochondrial network as expected, suggesting the reporter also works in *Drosophila* (Fig 11). However, it should be noted that the larvae did not pupariate, possibly due to a negative impact on normal development caused by high expression of the mt-Kaede-HI-NESS protein. Future efforts will need to be made to regulate the expression of mt-Kaede-HI-NESS, which can be accomplished using different weaker expressing driver lines.

Discussion

Building on the original HI-NESS genetic reporter for labeling DNA [37], we generated a modified mt-HI-NESS reporter that can be used for live cell imaging of mtDNA. Importantly, we show that when this construct is expressed at lower levels, it does not impair mtDNA replication or transcription, and thus will be a valuable tool to study mtDNA via live cell imaging. In addition, using the photoconvertible Kaede fluorescent protein, we show that the fluorescent protein domain can be swapped in the mt-HI-NESS reporter to make use of fluorescent proteins with different properties.

While the first iteration of the mt-mTagRFP-HI-NESS reporter was able to label mtDNA nucleoids, some unexpected non-nucleoid labelling of the mitochondrial network was observed. We demonstrated that the non-nucleoid signal was not due to overexpression, as it was also observed in cells expressing low levels of mt-TagRFP-HI-NESS. We suggest that the non-nucleoid signal is a result of poor DNA binding, which is reminiscent of the observations with the original

HI-NESS reporter when expressed in certain bacteria [37]. In this work, when the HI-NESS reporter was expressed in bacterial cells expressing endogenous H-NS, the HI-NESS reporter stained the bacterial cytosol, possibly because it was outcompeted by the full-length H-NS protein.

Despite the non-nucleoid signal in some cells, it is still possible to visualize mtDNA in live cells. Moreover, it is possible to identify cells that have specific nucleoid labelling. However, the reason why more specific labelling was observed in only certain cells within the same samples remains unclear. One way to circumvent this limitation is to only study cells without non-nucleoid staining. To this end, we showed that it is possible to select for cells that have specific mt-TagRFP-HI-NESS signal that colocalizes more strongly with mtDNA. Nonetheless, to improve the efficacy of nucleoid labelling, we generated a modified reporter with a second H-NS DNA binding domain, mt-TagRFP-N/C-HI-NESS, which has superior mtDNA specificity.

The fact that the non-specific mitochondrial labelling was only observed with the TagRFP fluorescent protein, and not the Kaede fluorescent protein was surprising. This observation suggests that there is something inherently different between the structures of these fluorescent proteins that impacts the ability of the H-NS domain to bind DNA. With respect to differences between the TagRFP and Kaede fluorescent proteins, they are 48% identical and 63.6% similar at the amino acid level. Notably, compared to Kaede, TagRFP has some amino acid insertions at the C-terminus (Fig S5), which is adjacent to the H-NS DNA binding domain. In this regard, it is also worth noting that the original HI-NESS DNA reporter used the mEOS3.2 fluorescent protein, which is more similar to the Kaede fluorescent protein at the C-terminus. It is also notable that TagRFP and Kaede have different tendencies to form oligomers, with TagRFP modified to reduce oligomerization [45], while Kaede is known to form tetramers [55]. Meanwhile, though mEos3.2 is listed as monomeric, it is notable that even monomeric fluorescent proteins can form oligomers under certain conditions [69]. Finally, the nucleoid specific labelling for mt-Kaede-HI-NESS may also be a result of clonal selection. Future work will more directly test the role of fluorescent protein oligomerization on the ability to modify DNA specificity. Regardless of the exact underlying mechanism for the non-specific nucleoid signal, this observation highlights the importance of carefully testing modified mt-HI-NESS reporters when different fluorescent proteins are substituted. If non-specific signal is

observed for a desired fluorescent protein, we would recommend testing it with the double N/C HI-NESS reporter backbone.

In the future we will work to develop additional mt-HI-NESS variants to take advantage of the variety of applications of various fluorescent proteins. However, when using the mt-HI-NESS reporters, it will be important to consider the specific fluorescent protein used, as well as to consider the possible effects of overexpression. As we have seen in budding yeast and flies, the issue of overexpression is also relevant in other organisms, but should be able to be mitigated. Nonetheless, that experimental conditions will likely need to be optimized and determined for each reporter in each model. Despite this potential limitation, we have shown that the mt-Kaede-HI-NESS can be used to study a variety of nucleoid dynamics including changes in size, number and distribution, as well as both cytosolic and extracellular release of mtDNA in live cell imaging experiments. These reporters will allow researchers to address questions about how nucleoids are distributed throughout the mitochondrial network, how mtDNA replication is coordinated with mitochondrial fission and fusion events, and to study the release of mtDNA into the cytosol or its endosomal/vesicle-mediated transport to autophagosomes for degradation [60,70,71]. As mtDNA release is increasingly recognized to occur in the context of human disease[72–74], better tools to study this process will be important. While our current efforts have focused on U2OS cells, we also plan to test the reporter in other human cell types. Beyond human cells, the mt-HI-NESS reporter can also be adapted to label mtDNA in other organisms including *A. thaliana* [64], *S. cerevisiae*, and *D. melanogaster*, and we expect it will be broadly applicable to several additional organisms.

Methods

Cell culture

HEK-293 and U2OS cells were cultured in Dulbecco's modified Eagle's medium (DMEM) (Gibco, 11965092) supplemented with 10% fetal bovine serum (FBS) (Fisher, 12483020). All cells were maintained at 37 °C and 5% CO2 incubator. The U2OS TFAM -/+ 1C11 line described previously [60], was a gift from Dr. Laura Newman (University of Virginia) and Dr. Gerald Shadel

(Salk Institute). U2OS MFN2 knockout cells were kindly gifted by Dr. Edward Fon (McGill University)[56]. For the mtDNA release studies, we added 20 µg/ml LPS for 12 hours (InvivoGen, tlrl-pb5lps) or 200 nM Dexamethasone (Sigma-Aldrich, D4902) for 18 hours to cells. Cells were subsequently imaged for mtDNA localization. Extra-mitochondrial DNA was analyzed using the mitoQC plugin on FIJI [75], while the mitochondrial network was quantified using MiNA [76].

Protein Structure Modeling

To model the predicted structures of our novel chimeric mt-HI-NESS proteins, we used Alphafold 2 [77,78] (https://colab.research.google.com/github/sokrypton/ColabFold/blob/main/beta/AlphaFold2_advanced.ipynb), and the 3D structures were visualized using Chimera software [79]. To model predicted interactions between our mt-HI-NESS proteins and mitochondrial DNA (mtDNA) we used the online application HADDOCK (YYY) [80]. The 3D co-ordinates of the mtDNA mitochondrial light strand promotor sequence (5'TTAACAGTCACCCCCCAACTAA3') were obtained from a previously reported crystal structure [81]. A range of active site residues YSYVDENGETKTWTGQGRTP was provided to the server based on previous reports [82] and all other parameters were set to default settings within the HADDOCK web application (https://wenmr.science.uu.nl/haddock2.4/). The complex with the highest binding energy score was used to generate the figures, which were visualized using the Chimera software.

HI-NESS plasmids

The mt-HI-NESS reporters were synthesized by VectorBuilder (Chicago, IL, USA) and cloned into a mammalian gene expression lentiviral vector following the hPGK Promoter. The vector contains ampicillin and puromycin resistance markers. Vector maps and DNA sequences are provided in the supplemental material, and the vector IDs, which can be used to retrieve detailed information about the vector of vectorbuilder.com are as follows:

mt-TagRFP-HI-NESS	VB221222-1228fqm
mt-TagRFP-N/C-HI-NESS	VB230529-1292kdj
mt-Kaede-HI-NESS	VB230322-1526htn

Lentivirus Production

HEK 293T were cells seeded into 100 mm dishes and incubated until they reached approximately 80% confluency. The plasmids containing mt-HI-NESS constructs (2µg) were transfected into HEK cells along with the packaging (psPAX2; 1.5 µg) and envelope (pMD2.G; 0.5 µg) plasmids using either FuGENE 6 or Lipofectamine 3000 transfection reagent (both from Invitrogen, Thermo Fisher Scientific, Burlington, Ontario, Canada) according to the manufacturer protocol. The medium was changed after cells were incubated at 37 °C and 5% CO2 for about 16 hrs. The culture medium containing lentivirus particles were collected at 48-96 hrs post-transfection.

Generation of stable cell lines

U2OS cells were seeded in a 6-well plate (50,000 cells/well) and cultured to reach 70% confluency (1-2 days). Fresh medium containing 8 µg/mL polybrene was added to cells, along with 100-500 µL of media containing lentivirus particles, for a total of 2 mL. Infected cells were incubated at 37 °C and 5% CO2 overnight at which point fresh culture medium without polybrene was added. After 24 hrs, the media was replaced again, this time containing puromycin (2 µg/mL) to select for stably transduced cells. Cells were grown for two weeks of selection, with puromycin-containing media changed every 2-3 days. To establish a genetically homogeneous population of cells, individual cells were obtained by serial dilution and single colonies picked.

Flow cytometry

Cells were sorted into four groups based on expression level of mTagRFP using a Sony SH800 cell sorter. Briefly, trypsinized, washed cells were suspended at a concentration of 1×10^6 cells/mL in the growth medium and filtered using a 40 µm cell strainer (VWR: 10199-655). Cells were then sorted into 15 mL collection tubes using a sterile 100 µm chip (Sony: LE-C3210).

Sample preparation for live-cell imaging

Unless otherwise indicated, all reagents and cell culture media components were obtained from ThermoFisher Scientific (Markham, Ontario, Canada). Transduced cells expressing different variants of the HI-NESS constructs were cultured in 35 mm dishes with a 1.5 glass coverslip bottom (Cellvis, D35-20-1.5-N). Imaging was performed either 1 or 2 days after seeding the cells in the dishes. For some experiments, an additional extrinsic fluorescent label was also applied to the cells (*e.g.*, SYBR Gold (S11494), MitoTracker Green FM (M7514) or MitoTracker Deep Red FM (M22426)). Stock solutions of each probe were prepared in sterile anhydrous DMSO (D12345) (stock concentrations: SYBR Gold 1:100; MitoTracker Green 1 mM; MitoTracker Deep Red 100 uM). To label the cells, media was aspirated, and fresh and pre-warmed media containing 1:1000 dilutions of SYBR Gold, MitoTracker Green, or MitoTracker Deep Red stock solutions were added. Cells were incubated for 1 hr, washed once with sterile PBS, and fresh media was then added to the wells. Cells were then imaged on an LCI system stage (Quorum Technologies, Guelph, Ontario, Canada), where temperature, humidity, and pH (5% CO2) were maintained.

Confocal live-cell imaging

Confocal images were acquired using a Nikon A1R system equipped with a Ti2 motorized microscope and Elements acquisition software version 5.42.01 and 5.42.03 (Nikon Canada, Mississauga, Ontario, Canada). The confocal system was equipped with lasers emitting at 405 nm (Ch1), 488 nm (Ch2), 562 nm (Ch3), and 639 nm (Ch4), and with standard PMTs (Ch1, Ch4) and GaAsP (Ch2, Ch3) detectors. Imaging was performed using a Plan Apo 60x 1.4 NA oil immersion lens. Spectral separation was effected using a primary dichroic (405/488/561/640) and additional filter cubes with center transmission wavelength and FWHM bandpass as follows (in nm): Ch1 452/45; 525/50; 595/50. One or more channels were selected, depending on the fluorophores used in the imaging experiment. Galvo-galvo scanning (unidirectional, 1.1 µs dwell time, sequential, laser switching per line) was used to record z-stacks at single time points. Lateral (x,y) sampling ranged from 0.1 to 0.3 mm, while axial sampling (z) ranged from 0.125 to 0.3 µm. The confocal pinhole diameters ranged from approximately 28 to 40 µm.

For imaging the photoconvertible Kaede variant, cells were labelled with MitoTracker Deep Red FM. Sequential images were acquired from Ch2 (green emission) and Ch3 (red emission) to monitor the shift in fluorescence emission green to red after activation with the 405 nm laser. The MitoTracker Deep Red FM fluorescence was monitored using Ch4 (far-red emission). Sequential Images were acquired 10 s for 2 min as a baseline. At 2 min, 405 nm laser was swept over a defined sub-cellular region-of-interest for 2 s. After the photostimulation pulse, images were acquired as for the baseline for up to 30 min. The 405 nm laser power was measured using the similar illumination conditions using a S170C sensor and PM100D power meter console (Thorlabs, NJ USA). A relative power of 5%, corresponding to 6.5 µW, was used to photoconvert the Kaede fusion protein. The laser exposure was about 6.5 µW x 2000 µs, for a total power of 13 µJ delivered to the region-of-interest (ROI). The photostimulated ROI had an area of 3.8 μm^2, corresponding to a power density of 340 $\mu J/cm^2$.

Western blotting

Cell pellets (~2,000,000 cells) were collected after trypsinization, washed with phosphate buffered saline (PBS) and lysed with RIPA buffer (ThermoFisherScientific, 89900) containing protease inhibitors. The cell lysates (20-50 µg of proteins) were resolved on SDS-PAGE gels (12%) and transferred onto PVDF Membranes in 25mM Tris, 192mM glycine and 20% (vol/vol) methanol at 30V overnight at 4°C. After blocking with 5% nonfat milk in TBST (25mM Tris, pH7.4, 150mM NaCl , 0.05% Tween-20), the blots were washed and incubated at RT for 2-3hrs with the following primary antibodies at the indicated dilutions; OxPhos antibody cocktail (Abcam, ab110411; 1:1000 dilution), anti-Actin (Sigma, A5316; 1:1000), anti-HSP60 (Cell Signaling Technology; 1:1000), anti-VDAC1 (Abcam, ab14734; 1:1000), anti-HA tag (Santa Cruz Biotechnology, sc-7392; 1:1000), and CD13 (homemade, clone AD-1 [63], diluted to 1 µg/ml). Appropriate horseradish peroxidase (HRP)-conjugated secondary antibodies were used as follows: goat anti-rabbit IgG HRP linked Antibody (Cell Signaling Technology, 7074S, 1:2000), or goat anti-mouse IgG HRP (Santa Cruz Biotechnology, sc-2055;1:2000). After washing with TBST (4x) the blots were developed with SuperSignal West Femto enhanced chemiluminescence

substrate (Pierce Chemical, Rockford, IL). The signal was detected and quantified with a chemiluminescence imaging analyzer (LAS3000 mini, Fujifilm).

Quantification of mtDNA copy number

Total DNA was isolated from cell pellets (~1,500,000 cells) using the E.Z.N.A. Tissue DNA Kit, Omega Bio-tek (VWR Scientific, D6905-03), according to the manufacturer's protocol. Isolated DNA (50-100 ng) was used for quantitative PCR (QPCR) to determine mtDNA copy number, as reported previously [16]. Primers used are as bellow: MT forward: CACCCAAGAACAGGGTTTGT; Reverse: TGGCCATGGGTATGTTGTTAA; 18S forward: TAGAGGGACAAGTGGCGTTC reverse:CGCTGAGCCAGTCAGTGT. Briefly, mtDNA and 18S DNA were amplified using PowerUp SYBR Green Master Mix (Thermo Fisher Scientific, A25742) in the QuantStudio 6 Flex Real-Time PCR system (Thermo Fisher Scientific) machine, and the delta delta Ct method was used to determine mtDNA copy number relative to the 18S. Reactions were performed in triplicate and mtDNA copy number analysis was performed on six independent biological replicates.

Quantification of mitochondrial RNA transcripts

RNA was isolated from cell pellets (~150,000 cells) using the E.Z.N.A. HP Total RNA Kit, Omega Bio-tek (VWR Scientific, CA101414-850), according to the manufacturer's protocol. Following isolation, cDNA was generated from 7.5 µg of RNA using the iScript™ Advanced cDNA Synthesis Kit (Biorad, 1725038), and 20-30 ng of cDNA was then used for quantitative PCR with PowerUp SYBR Green Master Mix (Thermo Fisher Scientific, A25742) in the QuantStudio 6 Flex Real-Time PCR system (Thermo Fisher Scientific) machine. The delta delta Ct method was used to determine the relative expression of various transcripts relative to actin using the primers indicated below:

COX I	Forward:	GACGTAGACACACGAGCATATTTCA
COX1	Reverse:	AGGACATAGTGGAAGTGAGCTACAAC
ND1	Forward:	AAGTCACCCTAGCCATCATTCTAC
ND1	Reverse	GCAGGAGTAATCAGAGGTGTTCTT

ATP6	Forward:	TAGCCATACACAACACTAAAGGACGA
ATP6	Reverse:	GGGCATTTTTAATCTTAGAGCGAAA
12S	Forward:	TAGAGGAGCCTGTTCTGTAATCGAT
12S	Reverse:	CGACCCTTAAGTTTCATAAGGGCTA
Actin	Forward:	AAGACCTGTACGCCAACACA
Actin	Reverse:	AGTACTTGCGCTCAGGAGGA

Reactions were performed in triplicate and three independent sample groups were tested. Data is presented as mean ± SD and unpaired, 2-tailed Student's t-tests were used to determine statistical significance.

Extracellular vesicles

For analysis of extracellular vesicles, cells were treated with 2 ug/ml LPS overnight, in serum-free media. For western blot and qPCR analysis pellets were extracted after ultracentrifugation at 100,000 g. For immunocapture and subsequent imaging, 20 mm live cell imaging dishes were coated overnight at 4 degrees with a homemade monoclonal antibody against CD13 (clone AD-1) [63]. After washing with PBS, the cell media supernatant (centrifuged for 2000 g for 20 minutes) was added to the antibody coated dish and incubated overnight at 4 degrees. The dishes were subsequently washed with PBS and the CD13(AD-1) mouse antibody prelabelled using Zenon antibody labelling kit Alexa Fluor 568 (Thermo Fisher Scientific, Z25006) was added to the dish. The coverslips were then imaged with confocal microscopy. Colocalization was performed using the JaCOP plugin on FIJI [83].

Yeast-specific methods

All strains were derived from W303, constructed using standard lithium acetate transformation, and verified by sequencing. Yeast strains used in this study are listed in Supplementary Table 1.

Microscopy

After inoculation in SCD (synthetic complete medium with 2% glucose), cells were grown for at least 24 hours while maintaining OD below 1 through appropriate dilutions. Coverslips (µ-Slide 8 Well, ibi-Treat, Ibidi) were covered with 200 µL concanavalin A (1 mg/mL), incubated for 5-10 min, and washed twice with double-distilled water. 1 mL of the cell culture was sonicated and 200 µL were transferred to a well. After about 5 min, the supernatant was removed, and cells were washed twice with filtered SCD. Finally, 200 µL filtered SCD was added to cover the wells.

Live cells were then imaged with a Zeiss LSM 800 confocal microscope, using a Plan-Apochromat 63x/1.4 NA Oil DIC objective and obtaining z-stacks of 46 slices with 0.22 µm increments. mKate2 was imaged with an excitation wavelength of 561 nm, detecting emission between 615 and 700 nm. mt-Kaede-HI-NESS was imaged with an excitation wavelength of 488 nm and detection between 410 and 546 nm. Bright-field images were obtained with the transmitted light detector (T-PMT).

Image analysis

Image analysis was performed using Cell-ACDC [84] and SpotMAX [67]. First, raw microscopy files were converted to TIFF using the Bioformats library [85]. Using the brightfield channel, cells were segmented with YeaZ v1.0.3 [86] embedded in Cell-ACDC. Segmentations were then carefully inspected and corrected where necessary, and mother-bud pairs were annotated.

To count the number of nucleoids and quantify the mitochondrial network volume, we used the software tool SpotMAX. The analysis is fully automatic and it was previously described [67]. The mitochondrial network volume was quantified by segmenting the mKate2 channel in 3D and summing the positive voxels. The analysis steps to segment the mitochondrial network are the following: 1) 3D Gaussian filter with sigma = 0.75, 2) 3D Sato filter to enhance the tubular structure with sigmas = (1.0, 2.0) [87], 3) automatic thresholding of the filtered image using the Yen algorithm [88], 4) connected-component labelling and removal of objects with less than 10 voxels volume (artefacts). To count the number of spots, we used SpotMAX with the Li algorithm [89] for semantic segmentation and local peak detection. Note that we distinguish between all detected spots (shown in Fig. S6) and high-confidence spots (shown in Fig. 10). The

high-confidence spots are those spots that pass the SpotMAX quality control consisting of two tests: a Welch's t-test and a minimum Glass' effect size between the Kaede and mKate2 normalised intensities within a spheroid with user-selected size centered at each spot. The spheroid radii were determined through visual inspection and they are 0.453 µm in the xy-directions (twice the Abbe's diffraction limit) and 1 µm in the z-direction. The valid spots are those where the t-statistic of the t-test is positive, the p-value is below 0.025, and the Glass's effect size is greater than 1.5. More details about this strategy can be found as published previously [67].

The signal-to-noise ratio (SNR) shown in Fig. S6C was calculated with the following formula:

$$(s_{mean}-b_{mean})/b_{std}$$

Here, s_{mean} is the mean of the raw pixel intensities inside the resolution-limited volume centered at each spot, and b_{mean} and b_{std} are the mean and the standard deviation of the background pixels, respectively. The background pixels are those inside the segmented mitochondrial network and outside the spots' masks. The spots' masks are constructed by placing a spheroid (with the same radii described above) on each detected spot (all spots).

mtDNA copy number quantification with qPCR

mtDNA copy numbers were determined largely following the strategy described previously [66]. After inoculation in SCD, cells were grown for at least 22 hours to a final OD between 0.1 and 0.5, always maintaining OD below 1 through appropriate dilutions. For each culture, 1 mL was sonicated and used to measure cell volume at a range of 10 to 328 fL using a Coulter counter (Beckman Coulter, Z2 Particle Counter), and another 1 mL was sonicated and used to determine bud fractions through visual inspection with a microscope (at least 200 cells were counted per replicate). For DNA extraction, 10 mL culture was centrifuged at 3434 g for 5 mins. The pellet was washed with 1 mL double-distilled water and centrifuged again for 1 min at 11600 g. The supernatant was removed, and pellets were frozen in liquid nitrogen and stored at -20°C.

DNA was extracted by phenol-chloroform-isoamyl alcohol (PCI) extraction. DNA pellets were resuspended in 200 µL DNA extraction buffer (2% Triton X-100, 1% SDS, 100 mM NaCl, 10 mM TRIS, 1 mM EDTA; pH = 8.0), and then 200 µL PCI and glass beads were added. Cells were mechanically disrupted by vortexing for 30 seconds at 3000 oscillations per minute (Mini-BeadBeater 24, 230 V, BioSpec Products). After centrifugation at 11600 g for 5 min, the aqueous phase was collected, and DNA was precipitated by mixing with 500 µL 100% ethanol and centrifugation at 11600 g for 5 min. Next, the pellet was washed with 700 µL 70% ethanol, and after complete removal and evaporation of the alcohol resuspended in 50 µL nuclease-free water. RNA residues were removed by 30 min incubation with RNase A (DNase-free; 1 mg/mL) at 37°C. PCI extraction was then repeated as described above. Finally, the DNA was resuspended in 50 µL nuclease-free water and stored at -20°C until further use.

To determine mtDNA concentrations, qPCRs were performed in technical triplicates using a LightCycler 480 Multiwell Plate 96 (Roche), using 1 ng DNA per replicate. A DNA-binding fluorescent dye (BioRad, SsoAdvanced Universal SYBR Green Supermix) and specific primers (Supplementary Table S2) for two nuclear DNA genes (*ACT1* and *MRX6*) and two mtDNA genes (*COX2* and *COX3*) were used. Single technical replicates were excluded from further analysis when the standard deviation between the three replicates was above 0.5. For each gene, Cq values of the remaining replicates were then averaged, and DNA concentrations were calculated using a linear fit to a gene-dependent calibration curve [66]. Concentrations of nuclear DNA and mtDNA were then calculated by averaging the concentrations of the respective genes. The ratio of mtDNA and nuclear DNA concentration was then used together with the average nuclear DNA copy number per cell as estimated from the bud fractions to calculate the average mtDNA copy number per cell [66].

Drosophila-specific methods

Drosophila husbandry

Drosophila stocks and experimental larvae were raised at room temperature on food consisting of 770 g Torula yeast, 1600 g cornmeal, 675 g sucrose, 2340 g D-glucose, 150 g agar, and 240 mL of an acid mixture (propionic acid/phosphoric acid) for every 34 L of water.

Drosophila stocks and genetics

For Drosophila experiments, da-Gal4 (BDSC #95282) line was crossed to UAS Kaede-HI-NESS (generated for this study). Hatched first instar larvae of the F1 progeny were then transferred into vials with food (50 larvae per vial). Experiments were conducted on larvae at 120 hrs after egg-laying (AEL).

Kaede HI-NESS stock generation

For Drosophila melanogaster studies, Kaede HI-NESS (from this paper) was cloned into a pDestination UAS-plasmid and purified plasmid was microinjected into flies carrying attP2 3L insertion sites to generate stable transgenic flies (injections were carried out by GENOMEPROLAB, Montreal, Canada).

Tissue Dissection, MitoTracker staining and Microscopy

Larvae (120hrs AEL) were inverted in Schneider's Drosophila medium (Gibco, 21720024) to expose the fat body. Inverted carcasses were incubated in in Schneider's media containing MitoTracker Deep Red (1:1000; Thermo Fisher Scientific, M22426) and Hoechst (1:5000; Thermo Fisher Scientific, 62249) for 30 minutes. Inverted larvae were then washed three times with schneider's media and fat body tissues were then immediately mounted in Vectasheild (Vector laboratories, H1000) mounting media on a glass coverslip and subsequently imaged.

Acknowledgements & Funding:

We would like to thank Dr. Laura Newman (University of Virginia), Dr. Gerald Shadel (Salk Institute), and Dr. Edward Fon (McGill University) for sharing CRISPR edited U2OS cell lines used in the studies. Work was supported by funds provided by a Natural Sciences and Engineering Research Council of Canada (NSERC) Discovery grant (TES) and a Crohn's & Colitis Canada Innovations grant (TES & PC). AJ was supported by a President's Doctoral Recruitment Scholarship in Transdisciplinary Research through the University of Calgary. We also thank the Cumming Medical Research Fund and the Snyder Institute for support of the imaging-based experiments. The funding sources were not involved in the study design, data collection and analysis, the writing of the report, nor in the decision to submit.

Conflict of interest statement:

The authors declare that they have no conflict of interest.

Author contributions:

JD designed, performed, and analyzed experiments, and prepared figures. LS designed, performed, and analyzed experiments, prepared figures, and edited the manuscript. MZ designed, performed, and analyzed experiments, and prepared figures. FS performed and analyzed experiments, prepared figures, and edited the manuscript. DB designed, performed, and analyzed experiments. FP performed image analysis, prepared figures and edited the manuscript. AB performed and analyzed experiments, and edited the manuscript. AS designed, performed, and analyzed experiments. AJ performed experiments and prepared figures. CB performed and analyzed experiments, and edited the manuscript. SG supervised the study. KS designed performed and analyzed experiments, supervised the study, wrote portions of the manuscript. PC conceived and designed the study, designed and analyzed experiments, supervised the study, prepared figures and wrote and revised the manuscript. TES conceived and designed the study, analyzed experiments, prepared figures, supervised the study, and wrote and revised the manuscript.

Figure Legends

Figure 1. Overview of mt-TagRFP-HI-NESS reporter. A) Depiction of the domain organization of the mt-TagRFP-HI-NESS protein. **B)** Predicted 3D structure of the mature protein in A generated with AlphaFold 2 bound to mtDNA as predicted via HADDOCK. Colours indicate mitochondrial targeting sequence (green), linker (black), TagRFP (red), H-NS DNA binding domain (blue), HA tag (yellow) and DNA (dark green).

Figure 2. mt-TagRFP-HI-NESS labels mtDNA nucleoids. A) U2OS cells transduced with mt-TagRFP-HI-NESS were imaged in the red channel and show variable RFP expression levels. U2OS cells transduced with mTagRFP and co-stained with SYBR Gold to label DNA (**B)** or MitoTracker Green to label mitochondrial networks (**C**), reveal that the mt-TagRFP protein localizes with mitochondrial nucleoids. Note some non-nucleoid mt-TagRFP-HI-NESS signal can be seen throughout the mitochondrial network in some cells (see arrowhead in B)

Figure 3. Clonal selection for improved mt-TagRFP-HI-NESS nucleoid imaging. Representative images from a selected clone U2OS cells transduced with mTag-RFP with more specific nucleoid staining as revealed by co-staining with SYBRGold to label DNA (**A**) or MitoTracker Green to label mitochondrial networks (**B**).

Figure 4. Characterization of mtDNA function. A) Immunoblotting of U2OS control cells, and cells sorted by flow cytometry for TagRFP expression into low, medium-low, medium-high and high groups. Blots were probed with the indicated antibodies. CI-CV denotes the specific oxidative phosphorylation complexes to which the indicated proteins belong. **B)** Quantitative PCR of mtDNA relative to 18S from the lines described in A, normalized to U2OS control (n=6 independent biological replicates). **C)** Quantitative RT-PCR of mtDNA-encoded transcripts (COX1, ND1, ATP6, 12S) relative to actin from the lines described in A and normalized to U2OS control. (N=3 independent biological replicates). Error bars represent SD. * denotes p-value<0.05 relative to WT cells, as determined via Student's T-test.

Figure 5. mt-TagRFP-N/C-HI-NESS labels mtDNA nucleoids. A) Depiction of the domain organization of the N/C and N/N double HI-NESS proteins. **B)** Predicted 3D structure of the mature proteins in A generated with AlphaFold 2 bound to mtDNA as predicted via HADDOCK.

Colours in A&B indicate mitochondrial targeting sequence (green), linker (black), TagRFP (red), H-NS DNA binding domain (blue), and HA tag (yellow). Representative images show improved mtDNA localization of mt-TagRFP-N/C-HI-NESS in U2OS cells co-stained with SYBR Gold to label DNA **(C)** or MitoTracker Green to label mitochondrial networks **(D)**.

Figure 6. mt-Kaede-HI-NESS labels mtDNA nucleoids. A) Depiction of the domain organization of the mt-Kaede-HI-NESS protein. **B)** Predicted 3D structure of the mature protein in A generated with AlphaFold 2 bound to mtDNA as predicted via HADDOCK. Colours in A&B indicate mitochondrial targeting sequence (green), linker (black), Kaede (red/green), H-NS DNA binding domain (blue), and HA tag (yellow). **C)** Representative image of U2OS cells transduced with mt-Kaede-N/C-HI-NESS and co-stained MitoTracker Deep Red to label mitochondrial networks reveals specific nucleoid signal. Moreover, 405 nm laser activation of a subregion, indicated by the dashed box, photoswitches a subset of the Kaede label, which can be used to follow specific nucleoids over time, as seen in the zoomed images **(D)**.

Figure 7: Transduction and transfection of U2OS WT and U2OS MFN2 KO cells using mt-Kaede-HI-NESS. A) Representative confocal images showing mitochondria (MitoTracker DeepRed) and mtDNA (mt-Kaede-HI-NESS) in transduced (WT U2OS) and transfected cell models (WT U2OS and U2OS MFN2 KO). **B-C)** Quantitative analyses of **(B)** number and **(C)** size of mtDNA nucleoids in transfected vs transduced cell models (U2OS WT/MFN2 KO). Colours indicate biological replicates, violins indicate median and interquartile range, multiple unpaired t-tests. Stats: ns $P > 0.05$; *$P \leq 0.05$; ****$P \leq 0.0001$.

Figure 8: Genetic and induced models of mitochondrial mtDNA release using mt-Kaede-HI-NESS. A) Representative confocal images showing mitochondria (MitoTracker Deep Red) and mtDNA (mt-Kaede-HI-NESS) in U2OS MFN2 knockout cells and U2OS TFAM 1C11 cells, circles indicate mtDNA not localized to the mitochondrial network. **B)** Quantitative analysis of number of mtDNA puncta not localized to the mitochondrial network, colours indicate biological replicates, lines indicate mean +/- SD, two-way ANOVA. **C-D)** Representative confocal images showing drug-induced extra-mitochondrial mtDNA, as shown by addition of **(C)** LPS and **(D)** Dexamethasone. **E-G)** Quantitative analyses of drug-based models of mtDNA release, showing

(E) number of nucleoids, **(F)** number of extra-mitochondrial nucleoids and (G) mean mitochondrial branch length. Colours indicate biological replicates, lines indicate mean +/- SD, two-way ANOVA. Stats: ns $P > 0.05$; ****$P \leq 0.0001$.

Figure 9: Extracellular mtDNA reported using mt-Kaede-HI-NESS. A) Schematic of the cell-free mtDNA detection assay. **B)** Representative confocal images showing mtDNA (mt-Kaede-HI-NESS) and extra-cellular vesicles (anti-CD13) in LPS treated and untreated cells, circles indicate presence of mtDNA. **C-H)** Quantification of extra-cellular mtDNA showing **(C)** Pearson's co-localization coefficient between green and magenta signals, number of **(D)** extra-cellular vesicles and **(E)** extra cellular mtDNA puncta, size of **(F)** extra-cellular vesicles and **(G)** extra cellular mtDNA puncta and (H) percentage of extracellular vesicles that contain mtDNA. All violins show median and interquartile range, unpaired t-test. **I)** Relative mtDNA copy number in the extracellular fraction for LPS treated and untreated cells, bars indicate mean +/- SD, unpaired t-test. **J)** Representative bands from western blot analysis of the extracellular fraction for LPS treated and untreated cells, showing relative protein amounts of CD-13 and HA-tag in LPS treated/untreated cells. Stats: *$P \leq 0.05$; **$P \leq 0.01$; ****$P \leq 0.0001$.

Figure 10: mt-Kaede-HI-NESS in *S. cerevisiae*. A) Schematic representation of the experimental setup. mt-Kaede-HI-NESS fused to a Su9 mitochondrial targeting sequence was expressed in budding yeast from promoters with varying strength. **B)** mtDNA copies per cell as determined by qPCR for strains expressing the mt-Kaede-HI-NESS reporter from different promoters as indicated. **C)** Number of automatically detected high-confidence spots (nucleoids, see methods) for budding yeast cells expressing mt-Kaede-HI-NESS from the *CUP1* or *ACT1* promoters, and corresponding *mip1Δ* cells. **D)** Corresponding representative confocal images (maximum projections) as well as automated network segmentation and detected nucleoids. In addition to mt-Kaede-HI-NESS, all strains express mKate2 targeted to the mitochondrial matrix for visualization of the mitochondrial network. Cell outlines and dashed lines connecting buds with their mother cells are shown in yellow. Automatic segmentation of the mitochondrial network is shown in blue. Automatically detected high-confidence spots (nucleoids) are shown in pink. In **C** and **D**, excitation intensities used to image mt-Kaede-HI-NESS were adjusted depending on the promoter to account for different expression levels. Scale bars denote 2 µm.

Figure 11: mt- Kaede-HI-NESS in *D. melanogaster* larval fat body. Representative confocal images of the larval fat body tissue from dau-Gal4 crossed to UAS- Kaede mt-HI-NESS. The mt-Kaede-HI-NESS (green) is localized within the mitochondrial network (magenta).

References

(1) Anderson, S.; Bankier, A. T.; Barrell, B. G.; de Bruijn, M. H.; Coulson, A. R.; Drouin, J.; Eperon, I. C.; Nierlich, D. P.; Roe, B. A.; Sanger, F.; Schreier, P. H.; Smith, A. J.; Staden, R.; Young, I. G. Sequence and Organization of the Human Mitochondrial Genome. *Nature* **1981**, *290* (5806), 457–465. https://doi.org/10.1038/290457a0.

(2) Kaufman, B. A.; Durisic, N.; Mativetsky, J. M.; Costantino, S.; Hancock, M. A.; Grutter, P.; Shoubridge, E. A. The Mitochondrial Transcription Factor TFAM Coordinates the Assembly of Multiple DNA Molecules into Nucleoid-like Structures. *Mol Biol Cell* **2007**, *18* (9), 3225–3236. https://doi.org/10.1091/mbc.E07-05-0404.

(3) Parisi, M. A.; Clayton, D. A. Similarity of Human Mitochondrial Transcription Factor 1 to High Mobility Group Proteins. *Science* **1991**, *252* (5008), 965–969. https://doi.org/10.1126/science.2035027.

(4) Kukat, C.; Wurm, C. A.; Spåhr, H.; Falkenberg, M.; Larsson, N.-G.; Jakobs, S. Super-Resolution Microscopy Reveals That Mammalian Mitochondrial Nucleoids Have a Uniform Size and Frequently Contain a Single Copy of mtDNA. *Proc Natl Acad Sci U S A* **2011**, *108* (33), 13534–13539. https://doi.org/10.1073/pnas.1109263108.

(5) Nicholls, T. J.; Gustafsson, C. M. Separating and Segregating the Human Mitochondrial Genome. *Trends Biochem Sci* **2018**, *43* (11), 869–881. https://doi.org/10.1016/j.tibs.2018.08.007.

(6) Chapman, J.; Ng, Y. S.; Nicholls, T. J. The Maintenance of Mitochondrial DNA Integrity and Dynamics by Mitochondrial Membranes. *Life (Basel)* **2020**, *10* (9). https://doi.org/10.3390/life10090164.

(7) Sabouny, R.; Shutt, T. E. The Role of Mitochondrial Dynamics in mtDNA Maintenance. *J Cell Sci* **2021**, *134* (24), jcs258944. https://doi.org/10.1242/jcs.258944.

(8) Semadhi, M. P.; Mulyaty, D.; Halimah, E.; Levita, J. Healthy Mitochondrial DNA in Balanced Mitochondrial Dynamics: A Potential Marker for Neuro aging Prediction (Review). *Biomed Rep* **2023**, *19* (3), 64. https://doi.org/10.3892/br.2023.1646.

(9) Lewis, S. C.; Uchiyama, L. F.; Nunnari, J. ER-Mitochondria Contacts Couple mtDNA Synthesis with Mitochondrial Division in Human Cells. *Science* **2016**, *353* (6296), aaf5549. https://doi.org/10.1126/science.aaf5549.

(10) Ilamathi, H. S.; Benhammouda, S.; Lounas, A.; Al-Naemi, K.; Desrochers-Goyette, J.; Lines, M. A.; Richard, F. J.; Vogel, J.; Germain, M. Contact Sites between Endoplasmic Reticulum Sheets and Mitochondria Regulate Mitochondrial DNA Replication and Segregation. *iScience* **2023**, *26* (7), 107180. https://doi.org/10.1016/j.isci.2023.107180.

(11) Silva Ramos, E.; Motori, E.; Bruser, C.; Kuhl, I.; Yeroslaviz, A.; Ruzzenente, B.; Kauppila, J. H. K.; Busch, J. D.; Hultenby, K.; Habermann, B. H.; Jakobs, S.; Larsson, N. G.; Mourier, A. Mitochondrial Fusion Is Required for Regulation of Mitochondrial DNA Replication. *PLoS Genet* **2019**, *15* (6), e1008085. https://doi.org/10.1371/journal.pgen.1008085.

(12) Ishihara, T.; Ban-Ishihara, R.; Maeda, M.; Matsunaga, Y.; Ichimura, A.; Kyogoku, S.; Aoki, H.; Katada, S.; Nakada, K.; Nomura, M.; Mizushima, N.; Mihara, K.; Ishihara, N. Dynamics of Mitochondrial DNA Nucleoids Regulated by Mitochondrial Fission Is Essential for Maintenance of Homogeneously Active Mitochondria during Neonatal Heart Development. *Mol Cell Biol* **2015**, *35* (1), 211–223. https://doi.org/10.1128/MCB.01054-14.

(13) Ban-Ishihara, R.; Ishihara, T.; Sasaki, N.; Mihara, K.; Ishihara, N. Dynamics of Nucleoid Structure Regulated by Mitochondrial Fission Contributes to Cristae Reformation and Release of Cytochrome c. *Proc Natl Acad Sci U S A* **2013**, *110* (29), 11863–11868. https://doi.org/10.1073/pnas.1301951110.

(14) Ilamathi, H. S.; Ouellet, M.; Sabouny, R.; Desrochers-Goyette, J.; Lines, M. A.; Pfeffer, G.; Shutt, T. E.; Germain, M. A New Automated Tool to Quantify Nucleoid Distribution within Mitochondrial Networks. *Sci Rep* **2021**, *11* (1), 22755. https://doi.org/10.1038/s41598-021-01987-9.
(15) Ishihara, T.; Ban-Ishihara, R.; Ota, A.; Ishihara, N. Mitochondrial Nucleoid Trafficking Regulated by the Inner-Membrane AAA-ATPase ATAD3A Modulates Respiratory Complex Formation. *Proc Natl Acad Sci U S A* **2022**, *119* (47), e2210730119. https://doi.org/10.1073/pnas.2210730119.
(16) Sabouny, R.; Wong, R.; Lee-Glover, L.; Greenway, S. C.; Sinasac, D. S.; Care4Rare Canada; Khan, A.; Shutt, T. E. Characterization of the C584R Variant in the mtDNA Depletion Syndrome Gene FBXL4, Reveals a Novel Role for FBXL4 as a Regulator of Mitochondrial Fusion. *Biochim Biophys Acta Mol Basis Dis* **2019**, *1865* (11), 165536. https://doi.org/10.1016/j.bbadis.2019.165536.
(17) Donkervoort, S.; Sabouny, R.; Yun, P.; Gauquelin, L.; Chao, K. R.; Hu, Y.; Al Khatib, I.; Töpf, A.; Mohassel, P.; Cummings, B. B.; Kaur, R.; Saade, D.; Moore, S. A.; Waddell, L. B.; Farrar, M. A.; Goodrich, J. K.; Uapinyoying, P.; Chan, S. H. S.; Javed, A.; Leach, M. E.; Karachunski, P.; Dalton, J.; Medne, L.; Harper, A.; Thompson, C.; Thiffault, I.; Specht, S.; Lamont, R. E.; Saunders, C.; Racher, H.; Bernier, F. P.; Mowat, D.; Witting, N.; Vissing, J.; Hanson, R.; Coffman, K. A.; Hainlen, M.; Parboosingh, J. S.; Carnevale, A.; Yoon, G.; Schnur, R. E.; Care4Rare Canada Consortium; Boycott, K. M.; Mah, J. K.; Straub, V.; Foley, A. R.; Innes, A. M.; Bönnemann, C. G.; Shutt, T. E. MSTO1 Mutations Cause mtDNA Depletion, Manifesting as Muscular Dystrophy with Cerebellar Involvement. *Acta Neuropathol* **2019**, *138* (6), 1013–1031. https://doi.org/10.1007/s00401-019-02059-z.
(18) Chen, H.; McCaffery, J. M.; Chan, D. C. Mitochondrial Fusion Protects against Neurodegeneration in the Cerebellum. *Cell* **2007**, *130* (3), 548–562. https://doi.org/10.1016/j.cell.2007.06.026.
(19) Newman, L. E.; Shadel, G. S. Mitochondrial DNA Release in Innate Immune Signaling. *Annu Rev Biochem* **2023**. https://doi.org/10.1146/annurev-biochem-032620-104401.
(20) Caicedo, A.; Benavides-Almeida, A.; Haro-Vinueza, A.; Peña-Cisneros, J.; Pérez-Meza, Á. A.; Michelson, J.; Peñaherrera, S.; Picard, M. Decoding the Nature and Complexity of Extracellular mtDNA: Types and Implications for Health and Disease. *Mitochondrion* **2024**, *75*, 101848. https://doi.org/10.1016/j.mito.2024.101848.
(21) Prole, D. L.; Chinnery, P. F.; Jones, N. S. Visualizing, Quantifying and Manipulating Mitochondrial DNA in Vivo. *J Biol Chem* **2020**. https://doi.org/10.1074/jbc.REV120.015101.
(22) Ashley, N.; Harris, D.; Poulton, J. Detection of Mitochondrial DNA Depletion in Living Human Cells Using PicoGreen Staining. *Exp Cell Res* **2005**, *303* (2), 432–446. https://doi.org/10.1016/j.yexcr.2004.10.013.
(23) Bereiter-Hahn, J.; Vöth, M. Distribution and Dynamics of Mitochondrial Nucleoids in Animal Cells in Culture. *EBO* **1996**, *1* (4), 1–17. https://doi.org/10.1007/s00898-996-0004-1.
(24) Jevtic, V.; Kindle, P.; Avilov, S. V. SYBR Gold Dye Enables Preferential Labelling of Mitochondrial Nucleoids and Their Time-Lapse Imaging by Structured Illumination Microscopy. *PLoS One* **2018**, *13* (9), e0203956. https://doi.org/10.1371/journal.pone.0203956.
(25) Jevtic, V.; Kindle, P.; Avilov, S. V. Specific Labeling of Mitochondrial Nucleoids for Time-Lapse Structured Illumination Microscopy. *J Vis Exp* **2020**, No. 160. https://doi.org/10.3791/60003.
(26) He, J.; Mao, C. C.; Reyes, A.; Sembongi, H.; Di Re, M.; Granycome, C.; Clippingdale, A. B.; Fearnley, I. M.; Harbour, M.; Robinson, A. J.; Reichelt, S.; Spelbrink, J. N.; Walker, J. E.; Holt, I. J. The AAA+ Protein ATAD3 Has Displacement Loop Binding Properties and Is Involved in Mitochondrial Nucleoid Organization. *J Cell Biol* **2007**, *176* (2), 141–146. https://doi.org/10.1083/jcb.200609158.
(27) Alexeyev, M. TFAM in mtDNA Homeostasis: Open Questions. *DNA (Basel)* **2023**, *3* (3), 134–136. https://doi.org/10.3390/dna3030011.

(28) Rajala, N.; Gerhold, J. M.; Martinsson, P.; Klymov, A.; Spelbrink, J. N. Replication Factors Transiently Associate with mtDNA at the Mitochondrial Inner Membrane to Facilitate Replication. *Nucleic Acids Res* **2014**, *42* (2), 952–967. https://doi.org/10.1093/nar/gkt988.
(29) Ekstrand, M. I.; Falkenberg, M.; Rantanen, A.; Park, C. B.; Gaspari, M.; Hultenby, K.; Rustin, P.; Gustafsson, C. M.; Larsson, N.-G. Mitochondrial Transcription Factor A Regulates mtDNA Copy Number in Mammals. *Hum Mol Genet* **2004**, *13* (9), 935–944. https://doi.org/10.1093/hmg/ddh109.
(30) Bonekamp, N. A.; Jiang, M.; Motori, E.; Villegas, R. G.; Koolmeister, C.; Atanassov, I.; Mesaros, A.; Park, C. B.; Larsson, N.-G. High Levels of TFAM Repress Mammalian Mitochondrial DNA Transcription in Vivo. *Life Science Alliance* **2021**, *4* (11). https://doi.org/10.26508/lsa.202101034.
(31) Ikeda, M.; Ide, T.; Fujino, T.; Arai, S.; Saku, K.; Kakino, T.; Tyynismaa, H.; Yamasaki, T.; Yamada, K.-I.; Kang, D.; Suomalainen, A.; Sunagawa, K. Overexpression of TFAM or Twinkle Increases mtDNA Copy Number and Facilitates Cardioprotection Associated with Limited Mitochondrial Oxidative Stress. *PLoS One* **2015**, *10* (3), e0119687. https://doi.org/10.1371/journal.pone.0119687.
(32) Ylikallio, E.; Tyynismaa, H.; Tsutsui, H.; Ide, T.; Suomalainen, A. High Mitochondrial DNA Copy Number Has Detrimental Effects in Mice. *Hum Mol Genet* **2010**, *19* (13), 2695–2705. https://doi.org/10.1093/hmg/ddq163.
(33) Sumitani, M.; Kasashima, K.; Ohta, E.; Kang, D.; Endo, H. Association of a Novel Mitochondrial Protein M19 with Mitochondrial Nucleoids. *J Biochem* **2009**, *146* (5), 725–732. https://doi.org/10.1093/jb/mvp118.
(34) Zhang, J.; Campbell, R. E.; Ting, A. Y.; Tsien, R. Y. Creating New Fluorescent Probes for Cell Biology. *Nat Rev Mol Cell Biol* **2002**, *3* (12), 906–918. https://doi.org/10.1038/nrm976.
(35) Cranfill, P. J.; Sell, B. R.; Baird, M. A.; Allen, J. R.; Lavagnino, Z.; de Gruiter, H. M.; Kremers, G.-J.; Davidson, M. W.; Ustione, A.; Piston, D. W. Quantitative Assessment of Fluorescent Proteins. *Nat Methods* **2016**, *13* (7), 557–562. https://doi.org/10.1038/nmeth.3891.
(36) Dairaghi, D. J.; Shadel, G. S.; Clayton, D. A. Human Mitochondrial Transcription Factor A and Promoter Spacing Integrity Are Required for Transcription Initiation. *Biochim Biophys Acta* **1995**, *1271* (1), 127–134. https://doi.org/10.1016/0925-4439(95)00019-z.
(37) Rashid, F.-Z. M.; Mahlandt, E.; van der Vaart, M.; Boer, D. E. C.; Varela Alvarez, M.; Henneman, B.; Brocken, D. J. W.; Voskamp, P.; Blok, A. J.; Shimizu, T. S.; Meijer, A. H.; Luijsterburg, M. S.; Goedhart, J.; Crémazy, F. G. E.; Dame, R. T. HI-NESS: A Family of Genetically Encoded DNA Labels Based on a Bacterial Nucleoid-Associated Protein. *Nucleic Acids Res* **2022**, *50* (2), e10. https://doi.org/10.1093/nar/gkab993.
(38) Shindo, H.; Iwaki, T.; Ieda, R.; Kurumizaka, H.; Ueguchi, C.; Mizuno, T.; Morikawa, S.; Nakamura, H.; Kuboniwa, H. Solution Structure of the DNA Binding Domain of a Nucleoid-Associated Protein, H-NS, from Escherichia Coli. *FEBS Lett* **1995**, *360* (2), 125–131. https://doi.org/10.1016/0014-5793(95)00079-o.
(39) Gordon, B. R. G.; Li, Y.; Cote, A.; Weirauch, M. T.; Ding, P.; Hughes, T. R.; Navarre, W. W.; Xia, B.; Liu, J. Structural Basis for Recognition of AT-Rich DNA by Unrelated Xenogeneic Silencing Proteins. *Proc Natl Acad Sci U S A* **2011**, *108* (26), 10690–10695. https://doi.org/10.1073/pnas.1102544108.
(40) Qin, L.; Erkelens, A. M.; Ben Bdira, F.; Dame, R. T. The Architects of Bacterial DNA Bridges: A Structurally and Functionally Conserved Family of Proteins. *Open Biol* **2019**, *9* (12), 190223. https://doi.org/10.1098/rsob.190223.
(41) Shutt, T. E.; Gray, M. W. Bacteriophage Origins of Mitochondrial Replication and Transcription Proteins. *Trends Genet* **2006**, *22* (2), 90–95. https://doi.org/10.1016/j.tig.2005.11.007.
(42) Shutt, T. E.; Gray, M. W. Homologs of Mitochondrial Transcription Factor B, Sparsely Distributed within the Eukaryotic Radiation, Are Likely Derived from the Dimethyladenosine Methyltransferase

of the Mitochondrial Endosymbiont. *Mol Biol Evol* **2006**, *23* (6), 1169–1179. https://doi.org/10.1093/molbev/msk001.

(43) Carrodeguas, J. A.; Kobayashi, R.; Lim, S. E.; Copeland, W. C.; Bogenhagen, D. F. The Accessory Subunit of Xenopus Laevis Mitochondrial DNA Polymerase Gamma Increases Processivity of the Catalytic Subunit of Human DNA Polymerase Gamma and Is Related to Class II Aminoacyl-tRNA Synthetases. *Mol Cell Biol* **1999**, *19* (6), 4039–4046. https://doi.org/10.1128/MCB.19.6.4039.

(44) Carrodeguas, J. A.; Bogenhagen, D. F. Protein Sequences Conserved in Prokaryotic Aminoacyl-tRNA Synthetases Are Important for the Activity of the Processivity Factor of Human Mitochondrial DNA Polymerase. *Nucleic Acids Res* **2000**, *28* (5), 1237–1244.

(45) Merzlyak, E. M.; Goedhart, J.; Shcherbo, D.; Bulina, M. E.; Shcheglov, A. S.; Fradkov, A. F.; Gaintzeva, A.; Lukyanov, K. A.; Lukyanov, S.; Gadella, T. W. J.; Chudakov, D. M. Bright Monomeric Red Fluorescent Protein with an Extended Fluorescence Lifetime. *Nat Methods* **2007**, *4* (7), 555–557. https://doi.org/10.1038/nmeth1062.

(46) Nooteboom, M.; Forkink, M.; Willems, P. H. G. M.; Koopman, W. J. H. Live-Cell Quantification of Mitochondrial Functional Parameters. In *Visualization Techniques: From Immunohistochemistry to Magnetic Resonance Imaging*; Badoer, E., Ed.; Neuromethods; Humana Press: Totowa, NJ, 2012; pp 111–127. https://doi.org/10.1007/978-1-61779-897-9_6.

(47) Ali, S. S.; Beckett, E.; Bae, S. J.; Navarre, W. W. The 5.5 Protein of Phage T7 Inhibits H-NS through Interactions with the Central Oligomerization Domain. *J Bacteriol* **2011**, *193* (18), 4881–4892. https://doi.org/10.1128/JB.05198-11.

(48) Forkink, M.; Smeitink, J. A. M.; Brock, R.; Willems, P. H. G. M.; Koopman, W. J. H. Detection and Manipulation of Mitochondrial Reactive Oxygen Species in Mammalian Cells. *Biochimica et Biophysica Acta (BBA) - Bioenergetics* **2010**, *1797* (6), 1034–1044. https://doi.org/10.1016/j.bbabio.2010.01.022.

(49) Filippin, L.; Abad, M. C.; Gastaldello, S.; Magalhães, P. J.; Sandonà, D.; Pozzan, T. Improved Strategies for the Delivery of GFP-Based Ca2+ Sensors into the Mitochondrial Matrix. *Cell Calcium* **2005**, *37* (2), 129–136. https://doi.org/10.1016/j.ceca.2004.08.002.

(50) Olenych, S. G.; Claxton, N. S.; Ottenberg, G. K.; Davidson, M. W. The Fluorescent Protein Color Palette. *Curr Protoc Cell Biol* **2007**, *Chapter 21*, Unit 21.5. https://doi.org/10.1002/0471143030.cb2105s36.

(51) Jumper, J.; Evans, R.; Pritzel, A.; Green, T.; Figurnov, M.; Ronneberger, O.; Tunyasuvunakool, K.; Bates, R.; Žídek, A.; Potapenko, A.; Bridgland, A.; Meyer, C.; Kohl, S. A. A.; Ballard, A. J.; Cowie, A.; Romera-Paredes, B.; Nikolov, S.; Jain, R.; Adler, J.; Back, T.; Petersen, S.; Reiman, D.; Clancy, E.; Zielinski, M.; Steinegger, M.; Pacholska, M.; Berghammer, T.; Bodenstein, S.; Silver, D.; Vinyals, O.; Senior, A. W.; Kavukcuoglu, K.; Kohli, P.; Hassabis, D. Highly Accurate Protein Structure Prediction with AlphaFold. *Nature* **2021**, *596* (7873), 583–589. https://doi.org/10.1038/s41586-021-03819-2.

(52) Wiedemann, N.; Pfanner, N. Mitochondrial Machineries for Protein Import and Assembly. *Annu Rev Biochem* **2017**, *86*, 685–714. https://doi.org/10.1146/annurev-biochem-060815-014352.

(53) Fukasawa, Y.; Tsuji, J.; Fu, S.-C.; Tomii, K.; Horton, P.; Imai, K. MitoFates: Improved Prediction of Mitochondrial Targeting Sequences and Their Cleavage Sites. *Mol Cell Proteomics* **2015**, *14* (4), 1113–1126. https://doi.org/10.1074/mcp.M114.043083.

(54) Almagro Armenteros, J. J.; Salvatore, M.; Emanuelsson, O.; Winther, O.; von Heijne, G.; Elofsson, A.; Nielsen, H. Detecting Sequence Signals in Targeting Peptides Using Deep Learning. *Life Sci Alliance* **2019**, *2* (5), e201900429. https://doi.org/10.26508/lsa.201900429.

(55) Ando, R.; Hama, H.; Yamamoto-Hino, M.; Mizuno, H.; Miyawaki, A. An Optical Marker Based on the UV-Induced Green-to-Red Photoconversion of a Fluorescent Protein. *Proc Natl Acad Sci U S A* **2002**, *99* (20), 12651–12656. https://doi.org/10.1073/pnas.202320599.

(56) Vranas, M.; Lu, Y.; Rasool, S.; Croteau, N.; Krett, J. D.; Sauvé, V.; Gehring, K.; Fon, E. A.; Durcan, T. M.; Trempe, J.-F. Selective Localization of Mfn2 near PINK1 Enables Its Preferential Ubiquitination by Parkin on Mitochondria. *Open Biol* **2022**, *12* (1), 210255. https://doi.org/10.1098/rsob.210255.
(57) Chen, H.; Vermulst, M.; Wang, Y. E.; Chomyn, A.; Prolla, T. A.; McCaffery, J. M.; Chan, D. C. Mitochondrial Fusion Is Required for mtDNA Stability in Skeletal Muscle and Tolerance of mtDNA Mutations. *Cell* **2010**, *141* (2), 280–289. https://doi.org/10.1016/j.cell.2010.02.026.
(58) Irazoki, A.; Gordaliza-Alaguero, I.; Frank, E.; Giakoumakis, N. N.; Seco, J.; Palacín, M.; Gumà, A.; Sylow, L.; Sebastián, D.; Zorzano, A. Disruption of Mitochondrial Dynamics Triggers Muscle Inflammation through Interorganellar Contacts and Mitochondrial DNA Mislocation. *Nat Commun* **2023**, *14* (1), 108. https://doi.org/10.1038/s41467-022-35732-1.
(59) West, A. P.; Khoury-Hanold, W.; Staron, M.; Tal, M. C.; Pineda, C. M.; Lang, S. M.; Bestwick, M.; Duguay, B. A.; Raimundo, N.; MacDuff, D. A.; Kaech, S. M.; Smiley, J. R.; Means, R. E.; Iwasaki, A.; Shadel, G. S. Mitochondrial DNA Stress Primes the Antiviral Innate Immune Response. *Nature* **2015**, *520* (7548), 553–557. https://doi.org/10.1038/nature14156.
(60) Newman, L. E.; Weiser Novak, S.; Rojas, G. R.; Tadepalle, N.; Schiavon, C. R.; Grotjahn, D. A.; Towers, C. G.; Tremblay, M.-È.; Donnelly, M. P.; Ghosh, S.; Medina, M.; Rocha, S.; Rodriguez-Enriquez, R.; Chevez, J. A.; Lemersal, I.; Manor, U.; Shadel, G. S. Mitochondrial DNA Replication Stress Triggers a Pro-Inflammatory Endosomal Pathway of Nucleoid Disposal. *Nat Cell Biol* **2024**. https://doi.org/10.1038/s41556-023-01343-1.
(61) Nguyen, M.; Collier, J. J.; Ignatenko, O.; Morin, G.; Huang, S.; Desjardins, M.; McBride, H. M. Parkinson's Genes Orchestrate Pyroptosis through Selective Trafficking of mtDNA to Leaky Lysosomes. bioRxiv September 12, 2023, p 2023.09.11.557213. https://doi.org/10.1101/2023.09.11.557213.
(62) Trumpff, C.; Marsland, A. L.; Basualto-Alarcón, C.; Martin, J. L.; Carroll, J. E.; Sturm, G.; Vincent, A. E.; Mosharov, E. V.; Gu, Z.; Kaufman, B. A.; Picard, M. Acute Psychological Stress Increases Serum Circulating Cell-Free Mitochondrial DNA. *Psychoneuroendocrinology* **2019**, *106*, 268–276. https://doi.org/10.1016/j.psyneuen.2019.03.026.
(63) Deng, J. T.; Hoylaerts, M. F.; Nouwen, E. J.; De Broe, M. E.; Van Hoof, V. O. Purification of Circulating Liver Plasma Membrane Fragments Using a Monoclonal Antileucine Aminopeptidase Antibody. *Hepatology* **1996**, *23* (3), 445–454. https://doi.org/10.1002/hep.510230308.
(64) Chustecki, J. M.; Schneider, A. Q.; Faber, M. H.; Christensen, A. C. Running on Empty: Mitochondria without mtDNA Exhibit Differential Motility and Connectivity. bioRxiv August 28, 2024, p 2024.08.27.609985. https://doi.org/10.1101/2024.08.27.609985.
(65) Keren, L.; Zackay, O.; Lotan-Pompan, M.; Barenholz, U.; Dekel, E.; Sasson, V.; Aidelberg, G.; Bren, A.; Zeevi, D.; Weinberger, A.; Alon, U.; Milo, R.; Segal, E. Promoters Maintain Their Relative Activity Levels under Different Growth Conditions. *Molecular Systems Biology* **2013**, *9* (1), 701. https://doi.org/10.1038/msb.2013.59.
(66) Seel, A.; Padovani, F.; Mayer, M.; Finster, A.; Bureik, D.; Thoma, F.; Osman, C.; Klecker, T.; Schmoller, K. M. Regulation with Cell Size Ensures Mitochondrial DNA Homeostasis during Cell Growth. *Nat Struct Mol Biol* **2023**. https://doi.org/10.1038/s41594-023-01091-8.
(67) Padovani, F.; Čavka, I.; Neves, A. R. R.; López, C. P.; Al-Refaie, N.; Bolcato, L.; Chatzitheodoridou, D.; Chadha, Y.; Su, X. A.; Lengefeld, J.; Cabianca, D. S.; Köhler, S.; Schmoller, K. M. SpotMAX: A Generalist Framework for Multi-Dimensional Automatic Spot Detection and Quantification. bioRxiv October 23, 2024, p 2024.10.22.619610. https://doi.org/10.1101/2024.10.22.619610.
(68) Osman, C.; Noriega, T. R.; Okreglak, V.; Fung, J. C.; Walter, P. Integrity of the Yeast Mitochondrial Genome, but Not Its Distribution and Inheritance, Relies on Mitochondrial Fission and Fusion. *Proc Natl Acad Sci U S A* **2015**, *112* (9), E947-956. https://doi.org/10.1073/pnas.1501737112.

(69) Zhang, M.; Chang, H.; Zhang, Y.; Yu, J.; Wu, L.; Ji, W.; Chen, J.; Liu, B.; Lu, J.; Liu, Y.; Zhang, J.; Xu, P.; Xu, T. Rational Design of True Monomeric and Bright Photoactivatable Fluorescent Proteins. *Nat Methods* **2012**, *9* (7), 727–729. https://doi.org/10.1038/nmeth.2021.
(70) Zecchini, V.; Paupe, V.; Herranz-Montoya, I.; Janssen, J.; Wortel, I. M. N.; Morris, J. L.; Ferguson, A.; Chowdury, S. R.; Segarra-Mondejar, M.; Costa, A. S. H.; Pereira, G. C.; Tronci, L.; Young, T.; Nikitopoulou, E.; Yang, M.; Bihary, D.; Caicci, F.; Nagashima, S.; Speed, A.; Bokea, K.; Baig, Z.; Samarajiwa, S.; Tran, M.; Mitchell, T.; Johnson, M.; Prudent, J.; Frezza, C. Fumarate Induces Vesicular Release of mtDNA to Drive Innate Immunity. *Nature* **2023**, *615* (7952), 499–506. https://doi.org/10.1038/s41586-023-05770-w.
(71) Sen, A.; Kallabis, S.; Gaedke, F.; Jüngst, C.; Boix, J.; Nüchel, J.; Maliphol, K.; Hofmann, J.; Schauss, A. C.; Krüger, M.; Wiesner, R. J.; Pla-Martín, D. Mitochondrial Membrane Proteins and VPS35 Orchestrate Selective Removal of mtDNA. *Nat Commun* **2022**, *13* (1), 6704. https://doi.org/10.1038/s41467-022-34205-9.
(72) Al Khatib, I.; Deng, J.; Lei, Y.; Torres-Odio, S.; Rojas, G. R.; Newman, L. E.; Chung, B. K.; Symes, A.; Zhang, H.; Huang, S.-Y. N.; Pommier, Y.; Khan, A.; Shadel, G. S.; West, A. P.; Gibson, W. T.; Shutt, T. E. Activation of the cGAS-STING Innate Immune Response in Cells with Deficient Mitochondrial Topoisomerase TOP1MT. *Hum Mol Genet* **2023**, ddad062. https://doi.org/10.1093/hmg/ddad062.
(73) Zaman, M.; Sharma, G.; Almutawa, W.; Soule, T. G.; Sabouny, R.; Joel, M.; Pfeffer, G.; Shutt, T. E. The MFN2 Q367H Variant from a Patient with Late-Onset Distal Myopathy Reveals a Novel Pathomechanism Connected to mtDNA-Mediated Inflammation. medRxiv June 21, 2024, p 2024.06.20.24309123. https://doi.org/10.1101/2024.06.20.24309123.
(74) VanPortfliet, J. J.; Chute, C.; Lei, Y.; Shutt, T. E.; West, A. P. Mitochondrial DNA Release and Sensing in Innate Immune Responses. *Hum Mol Genet* **2024**, *33* (R1), R80–R91. https://doi.org/10.1093/hmg/ddae031.
(75) Montava-Garriga, L.; Singh, F.; Ball, G.; Ganley, I. G. Semi-Automated Quantitation of Mitophagy in Cells and Tissues. *Mech Ageing Dev* **2020**, *185*, 111196. https://doi.org/10.1016/j.mad.2019.111196.
(76) Valente, A. J.; Maddalena, L. A.; Robb, E. L.; Moradi, F.; Stuart, J. A. A Simple ImageJ Macro Tool for Analyzing Mitochondrial Network Morphology in Mammalian Cell Culture. *Acta Histochem* **2017**, *119* (3), 315–326. https://doi.org/10.1016/j.acthis.2017.03.001.
(77) Jumper, J.; Evans, R.; Pritzel, A.; Green, T.; Figurnov, M.; Ronneberger, O.; Tunyasuvunakool, K.; Bates, R.; Žídek, A.; Potapenko, A.; Bridgland, A.; Meyer, C.; Kohl, S. A. A.; Ballard, A. J.; Cowie, A.; Romera-Paredes, B.; Nikolov, S.; Jain, R.; Adler, J.; Back, T.; Petersen, S.; Reiman, D.; Clancy, E.; Zielinski, M.; Steinegger, M.; Pacholska, M.; Berghammer, T.; Bodenstein, S.; Silver, D.; Vinyals, O.; Senior, A. W.; Kavukcuoglu, K.; Kohli, P.; Hassabis, D. Highly Accurate Protein Structure Prediction with AlphaFold. *Nature* **2021**, *596* (7873), 583–589. https://doi.org/10.1038/s41586-021-03819-2.
(78) Mirdita, M.; Schütze, K.; Moriwaki, Y.; Heo, L.; Ovchinnikov, S.; Steinegger, M. ColabFold: Making Protein Folding Accessible to All. *Nat Methods* **2022**, *19* (6), 679–682. https://doi.org/10.1038/s41592-022-01488-1.
(79) Pettersen, E. F.; Goddard, T. D.; Huang, C. C. UCSF Chimera—a visualization system for exploratory research and analysis. *J Comput Chem* **2004**, *25*, 1605–1612.
(80) van Zundert, G. C. P.; Rodrigues, J. P. G. L. M.; Trellet, M.; Schmitz, C.; Kastritis, P. L.; Karaca, E.; Melquiond, A. S. J.; van Dijk, M.; de Vries, S. J.; Bonvin, A. M. J. J. The HADDOCK2.2 Web Server: User-Friendly Integrative Modeling of Biomolecular Complexes. *Journal of Molecular Biology* **2016**, *428* (4), 720–725. https://doi.org/10.1016/j.jmb.2015.09.014.
(81) Choi, W. S.; Garcia-Diaz, M. A Minimal Motif for Sequence Recognition by Mitochondrial Transcription Factor A (TFAM). *Nucleic Acids Research* **2022**, *50* (1), 322–332. https://doi.org/10.1093/nar/gkab1230.

(82) Rosselli-Murai, L. K.; Sforça, M. L.; Sassonia, R. C.; Azzoni, A. R.; Murai, M. J.; de Souza, A. P.; Zeri, A. C. Structural Characterization of the H-NS Protein from Xylella Fastidiosa and Its Interaction with DNA. *Arch Biochem Biophys* **2012**, *526* (1), 22–28. https://doi.org/10.1016/j.abb.2012.06.007.
(83) Bolte, S.; Cordelières, F. P. A Guided Tour into Subcellular Colocalization Analysis in Light Microscopy. *J Microsc* **2006**, *224* (Pt 3), 213–232. https://doi.org/10.1111/j.1365-2818.2006.01706.x.
(84) Padovani, F.; Mairhörmann, B.; Falter-Braun, P.; Lengefeld, J.; Schmoller, K. M. Segmentation, Tracking and Cell Cycle Analysis of Live-Cell Imaging Data with Cell-ACDC. *BMC Biol* **2022**, *20* (1), 174. https://doi.org/10.1186/s12915-022-01372-6.
(85) Linkert, M.; Rueden, C. T.; Allan, C.; Burel, J.-M.; Moore, W.; Patterson, A.; Loranger, B.; Moore, J.; Neves, C.; MacDonald, D.; Tarkowska, A.; Sticco, C.; Hill, E.; Rossner, M.; Eliceiri, K. W.; Swedlow, J. R. Metadata Matters: Access to Image Data in the Real World. *Journal of Cell Biology* **2010**, *189* (5), 777–782. https://doi.org/10.1083/jcb.201004104.
(86) Dietler, N.; Minder, M.; Gligorovski, V.; Economou, A. M.; Joly, D. A. H. L.; Sadeghi, A.; Chan, C. H. M.; Koziński, M.; Weigert, M.; Bitbol, A.-F.; Rahi, S. J. A Convolutional Neural Network Segments Yeast Microscopy Images with High Accuracy. *Nat Commun* **2020**, *11* (1), 5723. https://doi.org/10.1038/s41467-020-19557-4.
(87) Sato, Y.; Nakajima, S.; Shiraga, N.; Atsumi, H.; Yoshida, S.; Koller, T.; Gerig, G.; Kikinis, R. Three-Dimensional Multi-Scale Line Filter for Segmentation and Visualization of Curvilinear Structures in Medical Images. *Med Image Anal* **1998**, *2* (2), 143–168. https://doi.org/10.1016/s1361-8415(98)80009-1.
(88) Yen, J.-C.; Chang, F.-J.; Chang, S. A New Criterion for Automatic Multilevel Thresholding. *IEEE Transactions on Image Processing* **1995**, *4* (3), 370–378. https://doi.org/10.1109/83.366472.
(89) Li, C. H.; Lee, C. K. Minimum Cross Entropy Thresholding. *Pattern Recognition* **1993**, *26* (4), 617–625. https://doi.org/10.1016/0031-3203(93)90115-D.

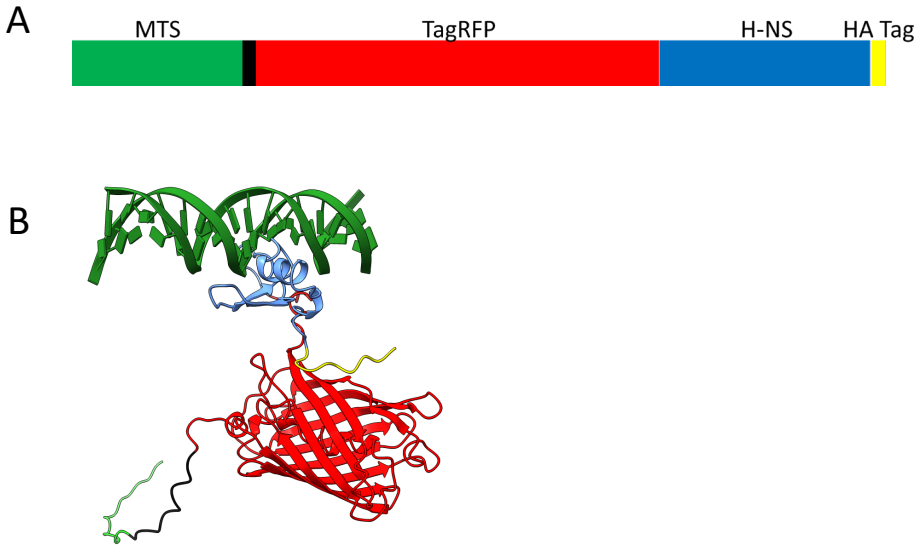

Figure 1. Overview of mt-TagRFP-HI-NESS reporter. A) Depiction of the domain organization of the mt-TagRFP-HI-NESS protein. **B)** Predicted 3D structure of the mature protein in A generated with AlphaFold 2 bound to mtDNA as predicted via HADDOCK. Colours indicate mitochondrial targeting sequence (green), linker (black), TagRFP (red), H-NS DNA binding domain (blue), HA tag (yellow) and DNA (dark green).

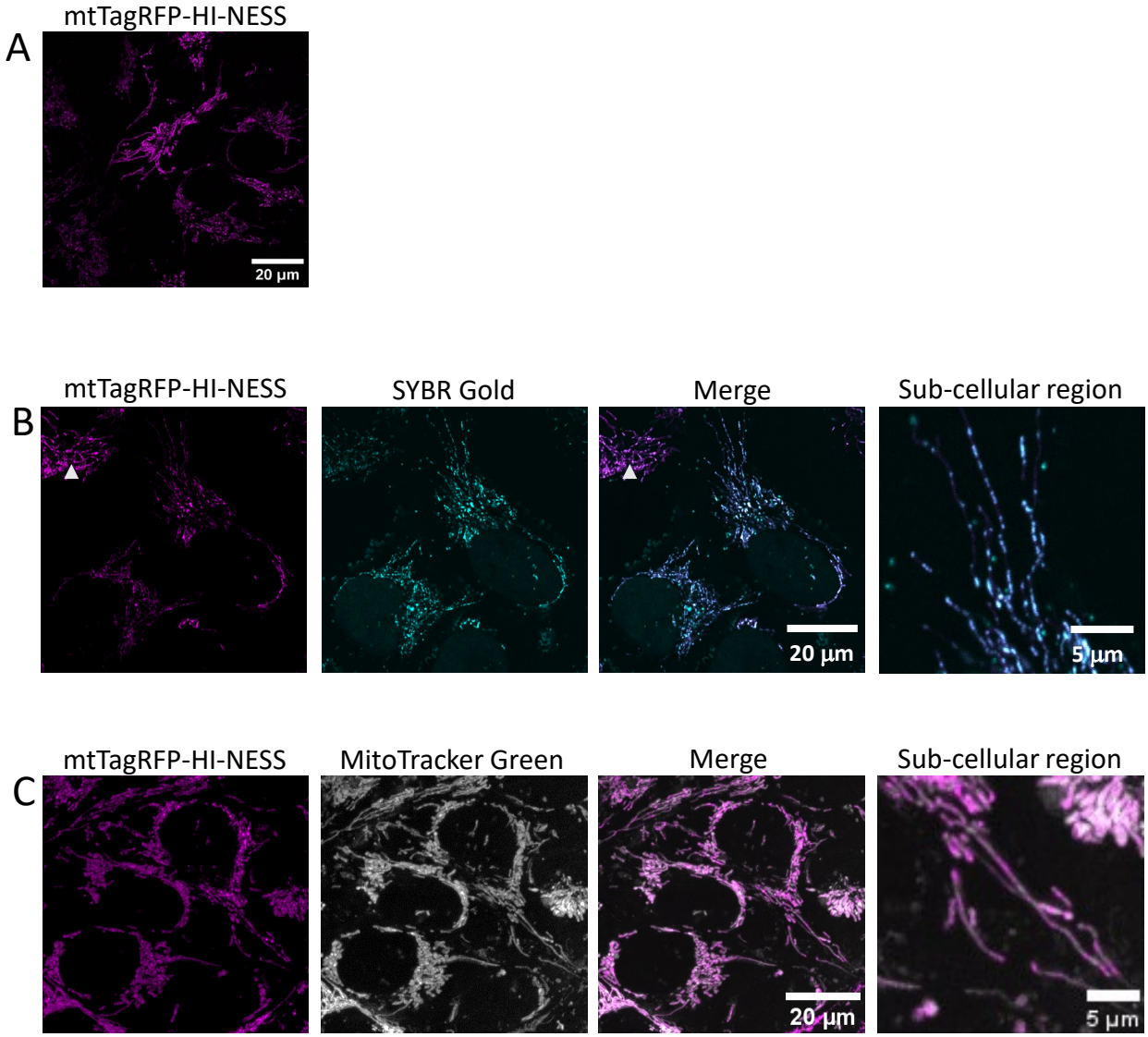

Figure 2. mt-TagRFP-HI-NESS labels mtDNA nucleoids. A) U2OS cells transduced with mt-TagRFP-HI-NESS were imaged in the red channel and show variable RFP expression levels. U2OS cells transduced with mTagRFP and co-stained with SYBR Gold to label DNA (**B)** or MitoTracker Green to label mitochondrial networks (**C**), reveal that the mt-TagRFP protein localizes with mitochondrial nucleoids. Note some non-nucleoid mt-TagRFP-HI-NESS signal can be seen throughout the mitochondrial network in some cells (see arrowhead in B)

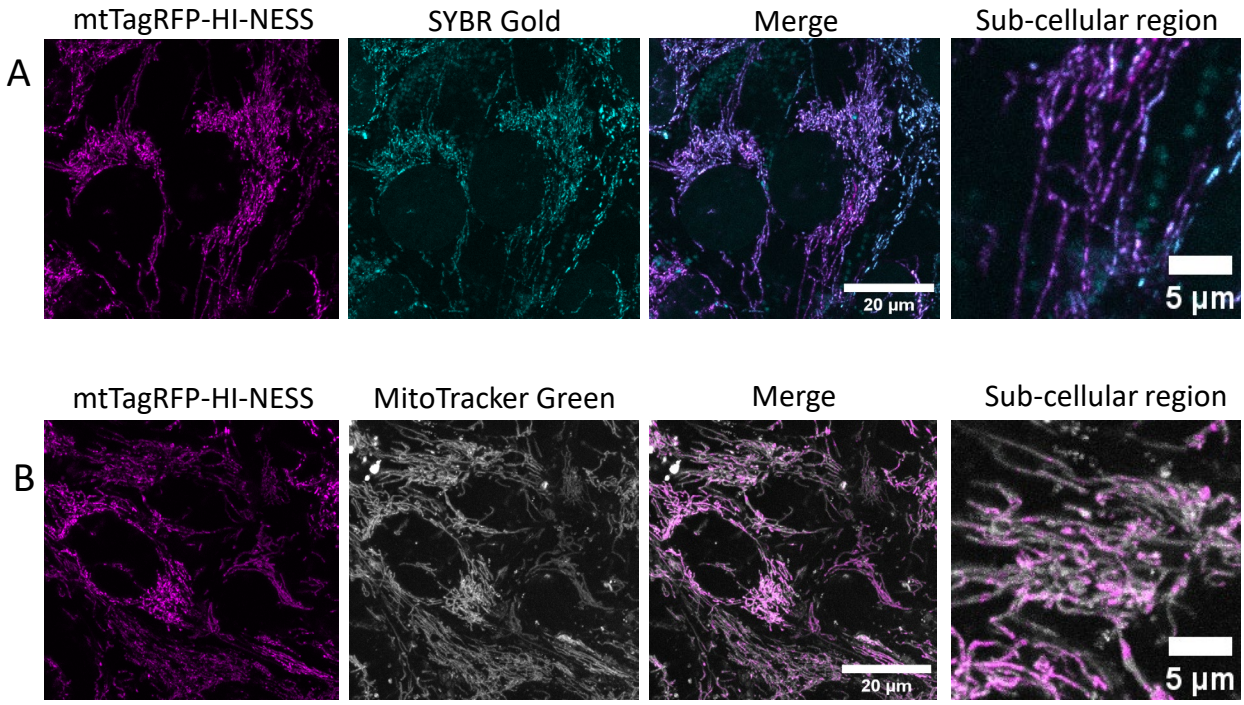

Figure 3. Clonal selection for improved mt-TagRFP-HI-NESS nucleoid imaging. Representative images from a selected clone U2OS cells transduced with mTag-RFP with more specific nucleoid staining as revealed by co-staining with SYBRGold to label DNA (**A**) or MitoTracker Green to label mitochondrial networks (**B**).

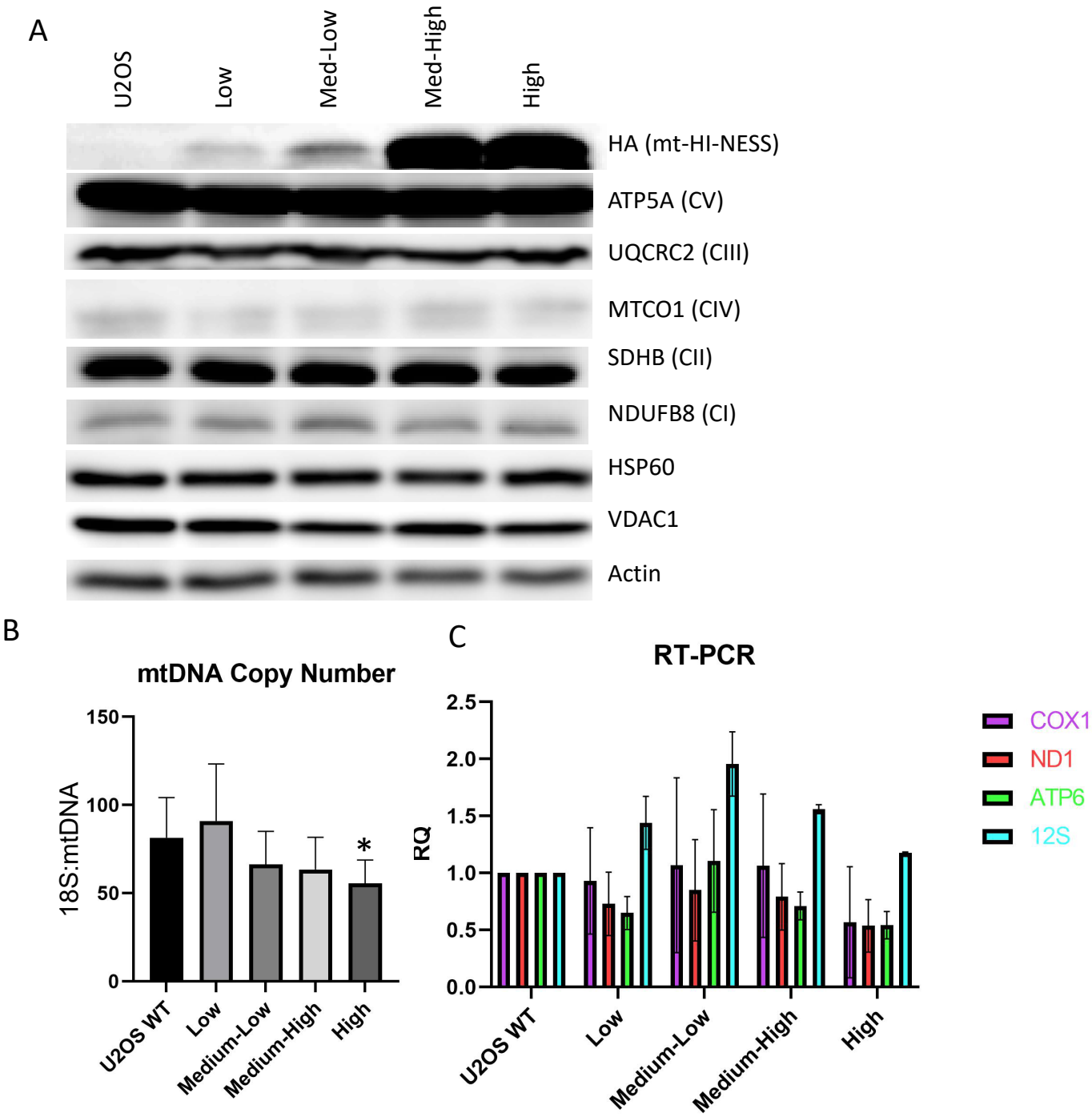

Figure 4. Characterization of mtDNA function. A) Immunoblotting of U2OS control cells, and cells sorted by flow cytometry for TagRFP expression into low, medium-low, medium-high and high groups. Blots were probed with the indicated antibodies. CI-CV denotes the specific oxidative phosphorylation complexes to which the indicated proteins belong. **B)** Quantitative PCR of mtDNA relative to 18S from the lines described in A, normalized to U2OS control (n=6 independent biological replicates). **C)** Quantitative RT-PCR of mtDNA-encoded transcripts (COX1, ND1, ATP6, 12S) relative to actin from the lines described in A and normalized to U2OS control. (N=3 independent biological replicates). Error bars represent SD. * denotes p-value<0.05 relative to WT cells, as determined via Student's T-test.

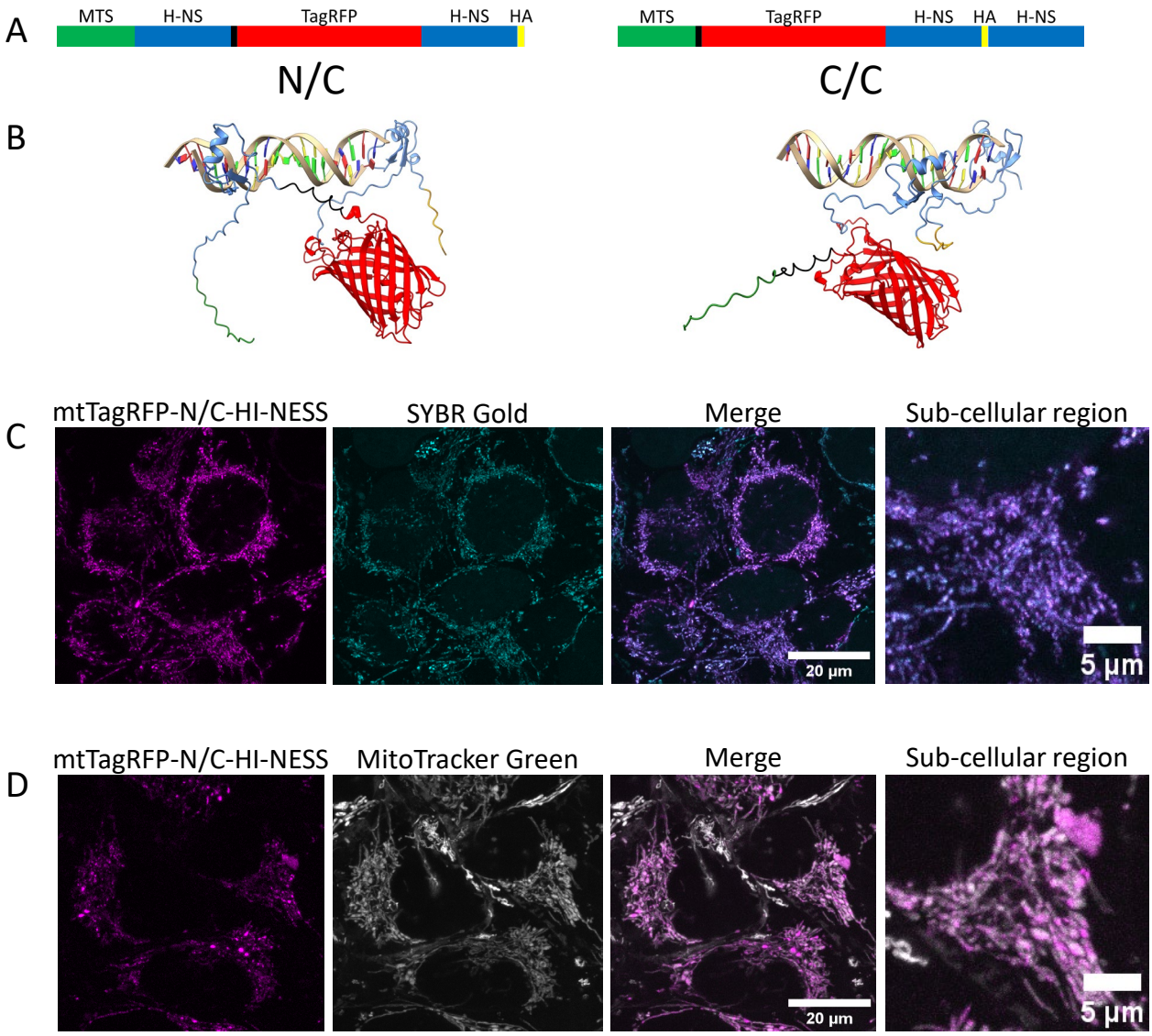

Figure 5. mt-TagRFP-N/C-HI-NESS labels mtDNA nucleoids. A) Depiction of the domain organization of the N/C and N/N double HI-NESS proteins. **B)** Predicted 3D structure of the mature proteins in A generated with AlphaFold 2 bound to mtDNA as predicted via HADDOCK. Colours in A&B indicate mitochondrial targeting sequence (green), linker (black), TagRFP (red), H-NS DNA binding domain (blue), and HA tag (yellow). Representative images show improved mtDNA localization of mt-TagRFP-N/C-HI-NESS in U2OS cells co-stained with SYBR Gold to label DNA **(C)** or MitoTracker Green to label mitochondrial networks **(D)**.

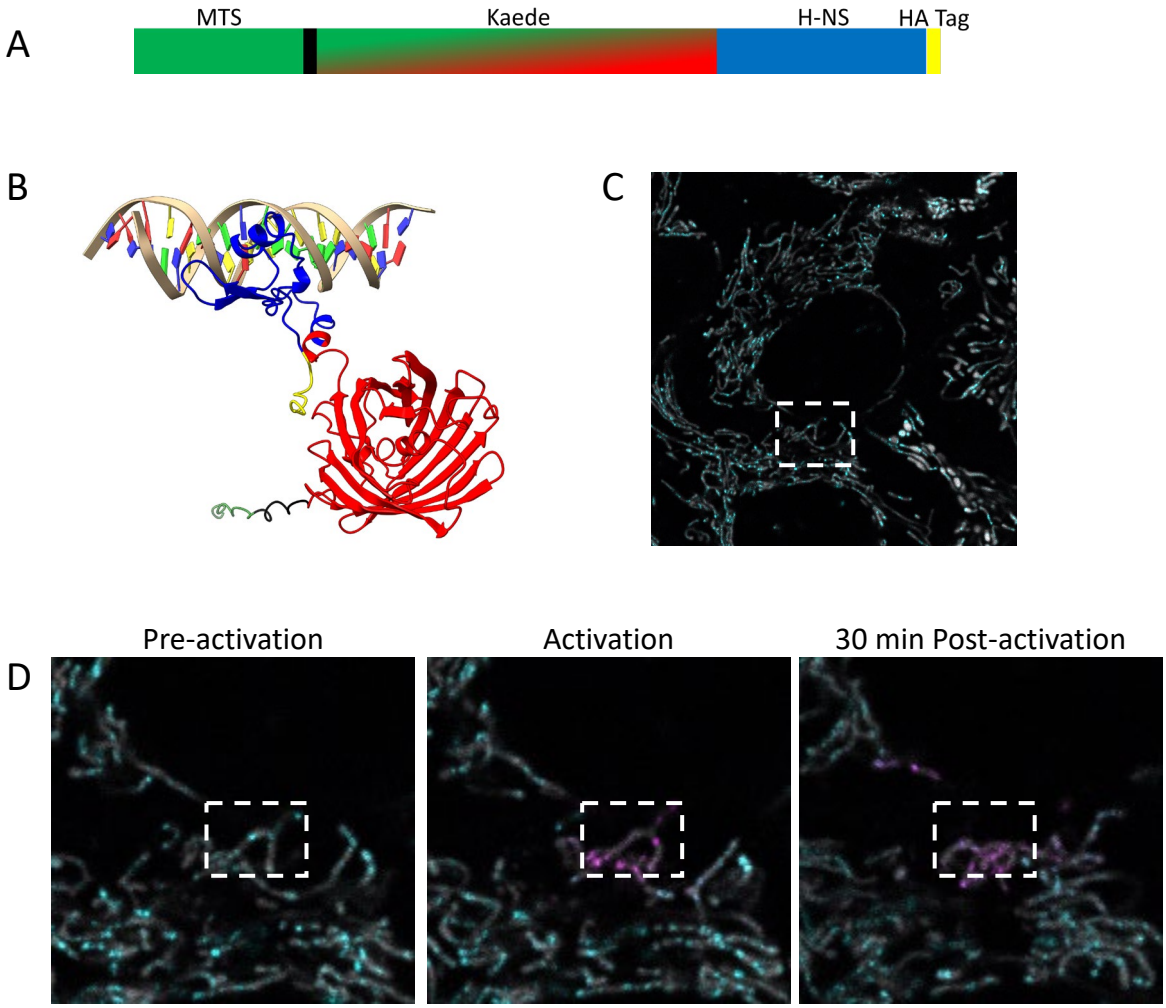

Figure 6. mt-Kaede-HI-NESS labels mtDNA nucleoids. A) Depiction of the domain organization of the mt-Kaede-HI-NESS protein. **B)** Predicted 3D structure of the mature protein in A generated with AlphaFold 2 bound to mtDNA as predicted via HADDOCK. Colours in A&B indicate mitochondrial targeting sequence (green), linker (black), Kaede (red/green), H-NS DNA binding domain (blue), and HA tag (yellow). **C**) Representative image of U2OS cells transduced with mt-Kaede-N/C-HI-NESS and co-stained MitoTracker Deep Red to label mitochondrial networks reveals specfic nucleoid signal. Moreover, 405nm laser activation of a subregion, indicated by the dashed box, photoswitches a subset of the Kaede label, which can be used to follow specific nucleoids over time, as seen in the zoomed images (**D**).

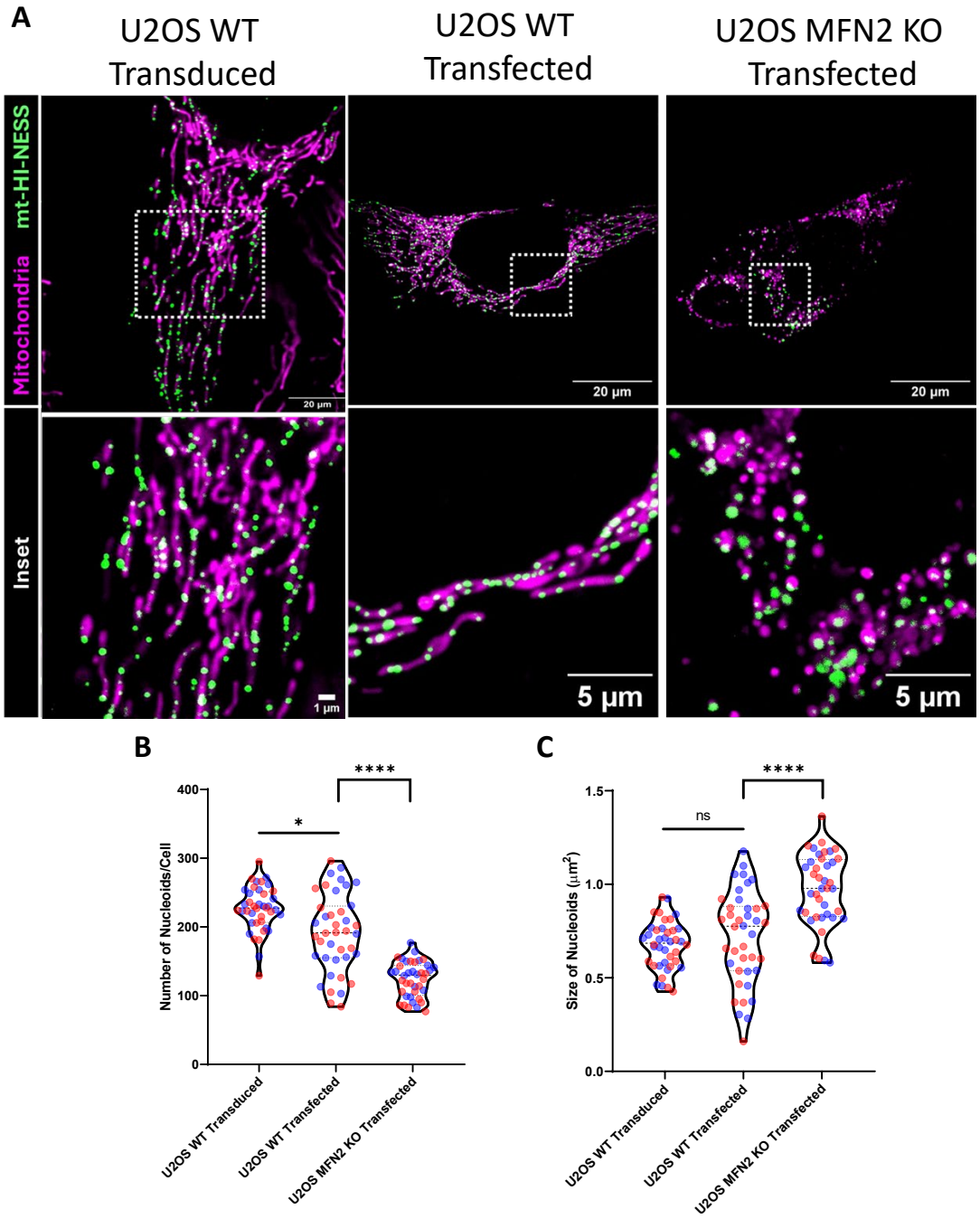

Figure 7: Transduction and transfection of U2OS WT and U2OS MFN2 KO cells using mt-Kaede-HI-NESS. A) Representative confocal images showing mitochondria (MitoTracker DeepRed) and mtDNA (mt-Kaede-HI-NESS) in transduced (WT U2OS) and transfected cell models (WT U2OS and U2OS MFN2 KO). **B-C)** Quantitative analyses of **(B)** number and **(C)** size of mtDNA nucleoids in transfected vs transduced cell models (U2OS WT/MFN2 KO). Colours indicate biological replicates, violins indicate median and interquartile range, multiple unpaired t-tests. Stats: ns $P > 0.05$; *$P \leq 0.05$; ****$P \leq 0.0001$.

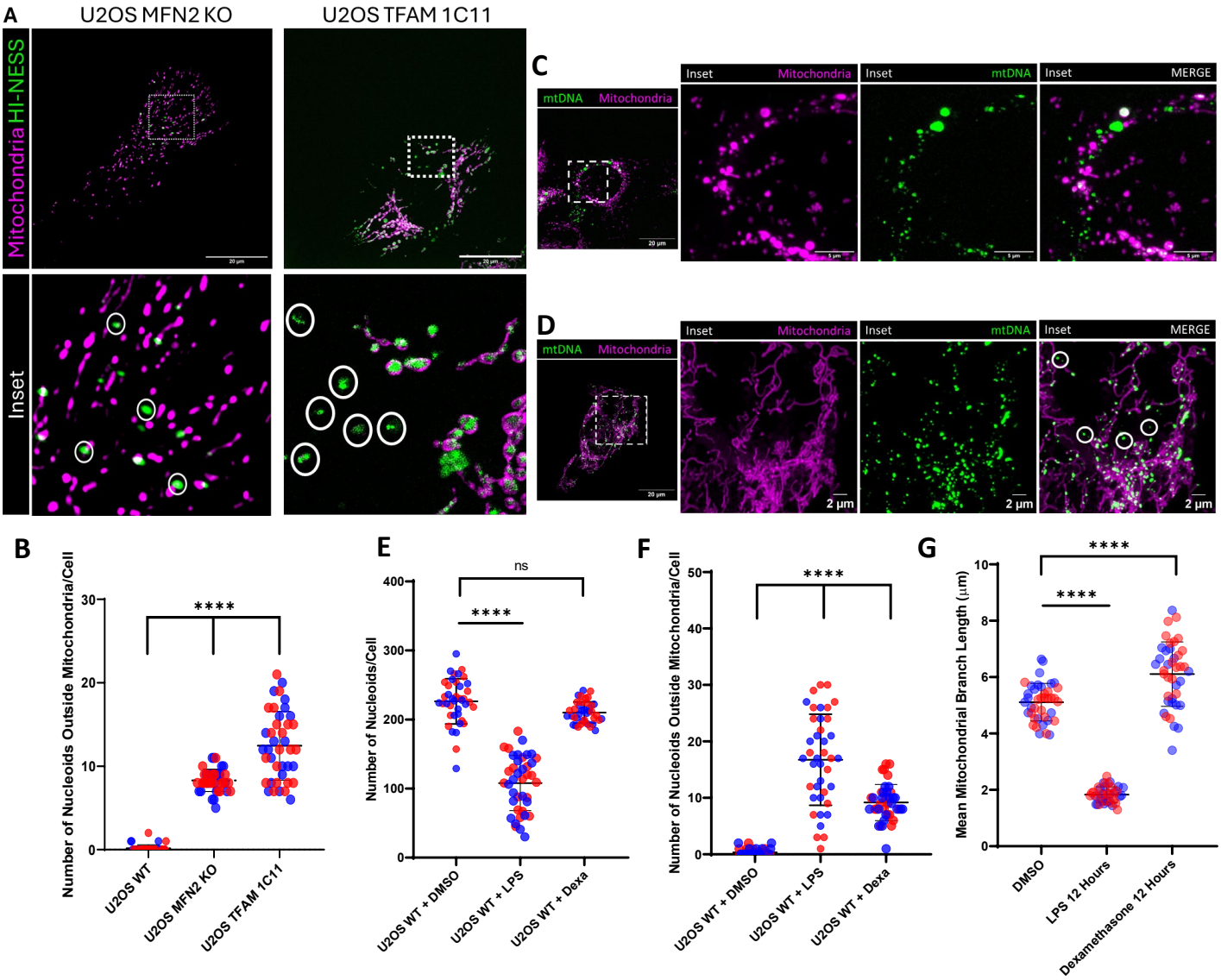

Figure 8: Genetic and induced models of mitochondrial mtDNA release using mt-Kaede-HI-NESS. A) Representative confocal images showing mitochondria (MitoTracker Deep Red) and mtDNA (mt-Kaede-HI-NESS) in U2OS MFN2 knockout cells and U2OS TFAM 1C11 cells, circles indicate mtDNA not localized to the mitochondrial network. **B)** Quantitative analysis of number of mtDNA puncta not localized to the mitochondrial network, colours indicate biological replicates, lines indicate mean +/- SD, two-way ANOVA. **C-D)** Representative confocal images showing drug-induced extra-mitochondrial mtDNA, as shown by addition of **(C)** LPS and **(D)** Dexamethasone. **E-G)** Quantitative analyses of drug-based models of mtDNA release, showing **(E)** number of nucleoids, **(F)** number of extra-mitochondrial nucleoids and (G) mean mitochondrial branch length. Colours indicate biological replicates, lines indicate mean +/- SD, two-way ANOVA. Stats: ns $P > 0.05$; ****$P \leq 0.0001$.

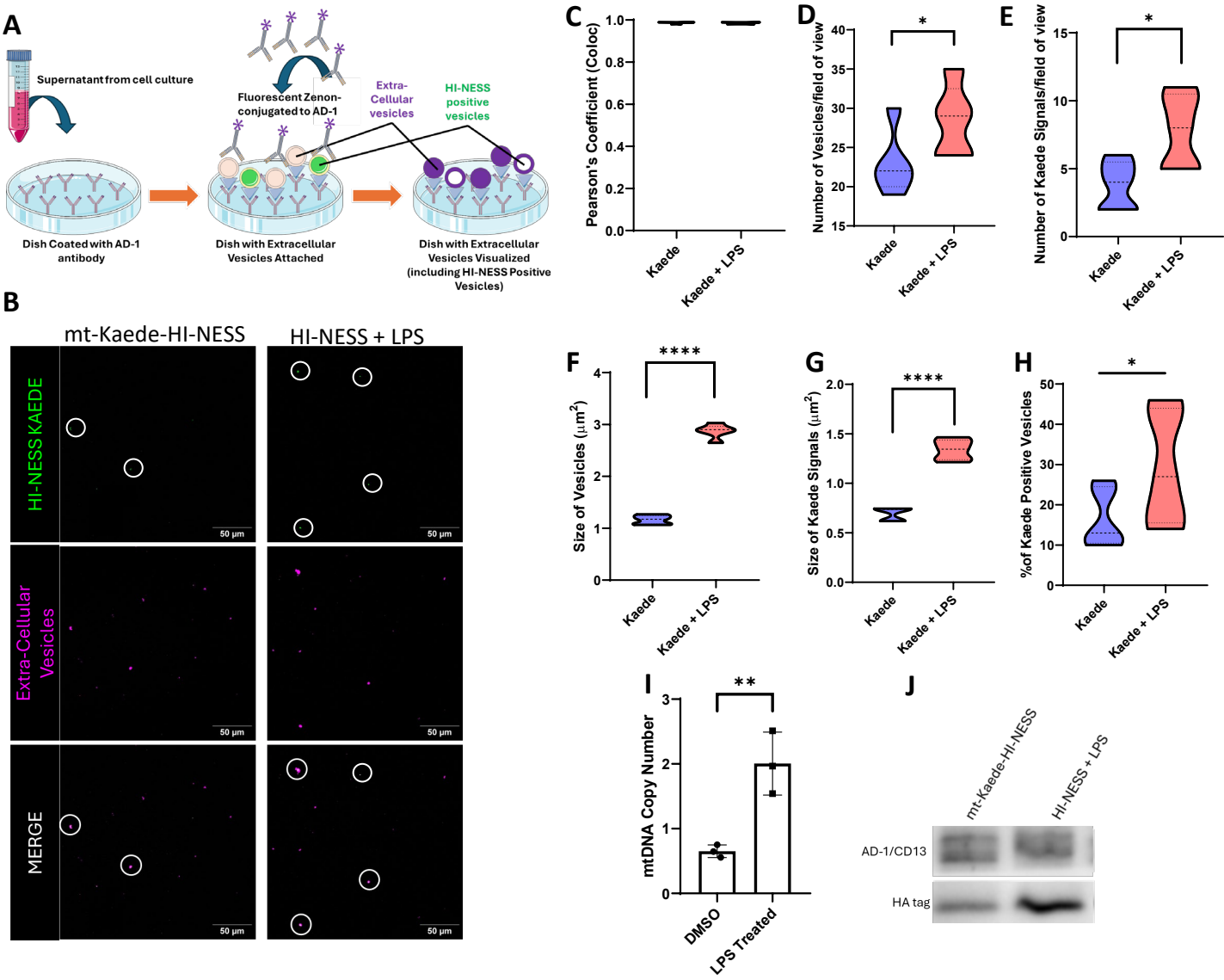

Figure 9: Extracellular mtDNA reported using mt-Kaede-HI-NESS. A) Schematic of the cell-free mtDNA detection assay. **B)** Representative confocal images showing mtDNA (mt-Kaede-HI-NESS) and extra-cellular vesicles (anti-CD13) in LPS treated and untreated cells, circles indicate presence of mtDNA. **C-H)** Quantification of extra-cellular mtDNA showing **(C)** Pearson's co-localization coefficient between green and magenta signals, number of **(D)** extra-cellular vesicles and **(E)** extra cellular mtDNA puncta, size of **(F)** extra-cellular vesicles and **(G)** extra cellular mtDNA puncta and (H) percentage of extracellular vesicles that contain mtDNA. All violins show median and interquartile range, unpaired t-test. **I)** Relative mtDNA copy number in the extracellular fraction for LPS treated and untreated cells, bars indicate mean +/- SD, unpaired t-test. **J)** Representative bands from western blot analysis of the extracellular fraction for LPS treated and untreated cells, showing relative protein amounts of CD-13 and HA-tag in LPS treated/untreated cells. Stats: *P ≤ 0.05; **P ≤ 0.01; ****P ≤ 0.0001.

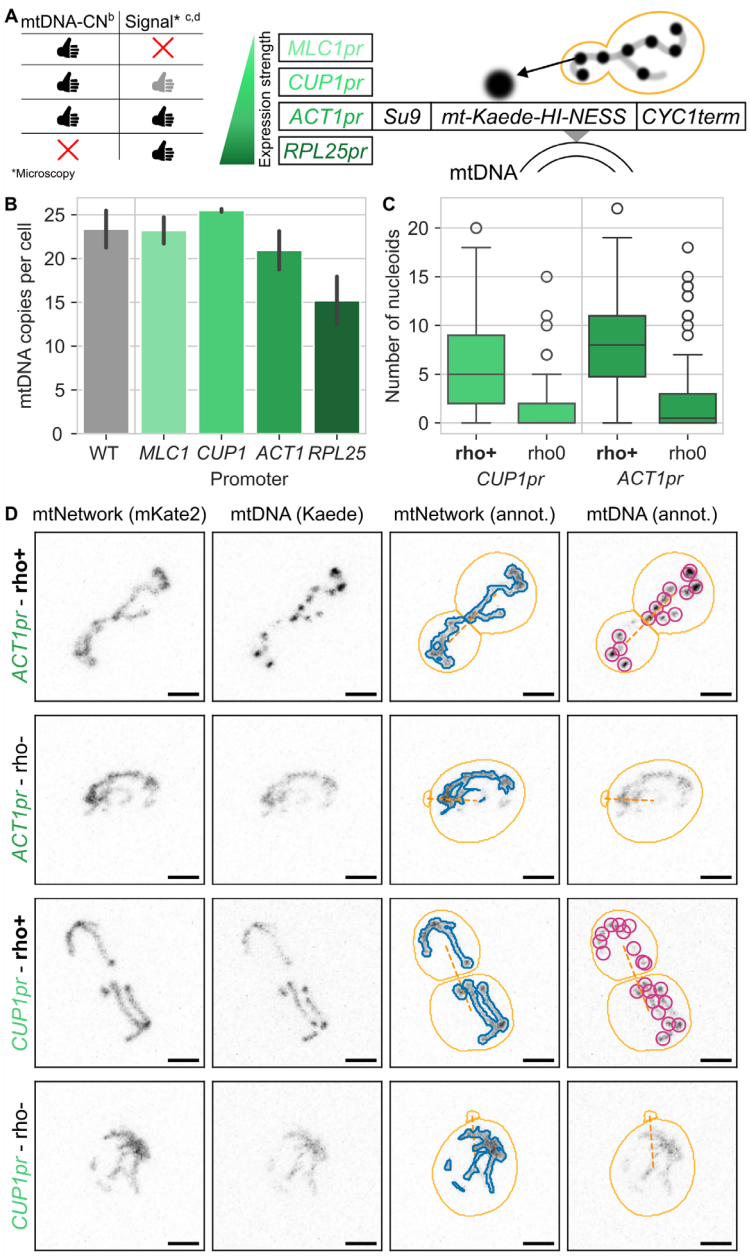

Figure 10: mt-Kaede-HI-NESS in *S. cerevisiae*. A) Schematic representation of the experimental setup. mt-Kaede-HI-NESS fused to a Su9 mitochondrial targeting sequence was expressed in budding yeast from promoters with varying strength. **B)** mtDNA copies per cell as determined by qPCR for strains expressing the mt-Kaede-HI-NESS reporter from different promoters as indicated. **C)** Number of automatically detected high-confidence spots (nucleoids, see methods) for budding yeast cells expressing mt-Kaede-HI-NESS from the *CUP1* or *ACT1* promoters, and corresponding *mip1Δ* cells. **D)** Corresponding representative confocal images (maximum projections) as well as automated network segmentation and detected nucleoids. In addition to mt-Kaede-HI-NESS, all strains express mKate2 targeted to the mitochondrial matrix for visualization of the mitochondrial network. Cell outlines and dashed lines connecting buds with their mother cells are shown in yellow. Automatic segmentation of the mitochondrial network is shown in blue. Automatically detected high-confidence spots (nucleoids) are shown in pink. In **C** and **D**, excitation intensities used to image mt-Kaede-HI-NESS were adjusted depending on the promoter to account for different expression levels. Scale bars denote 2 µm.

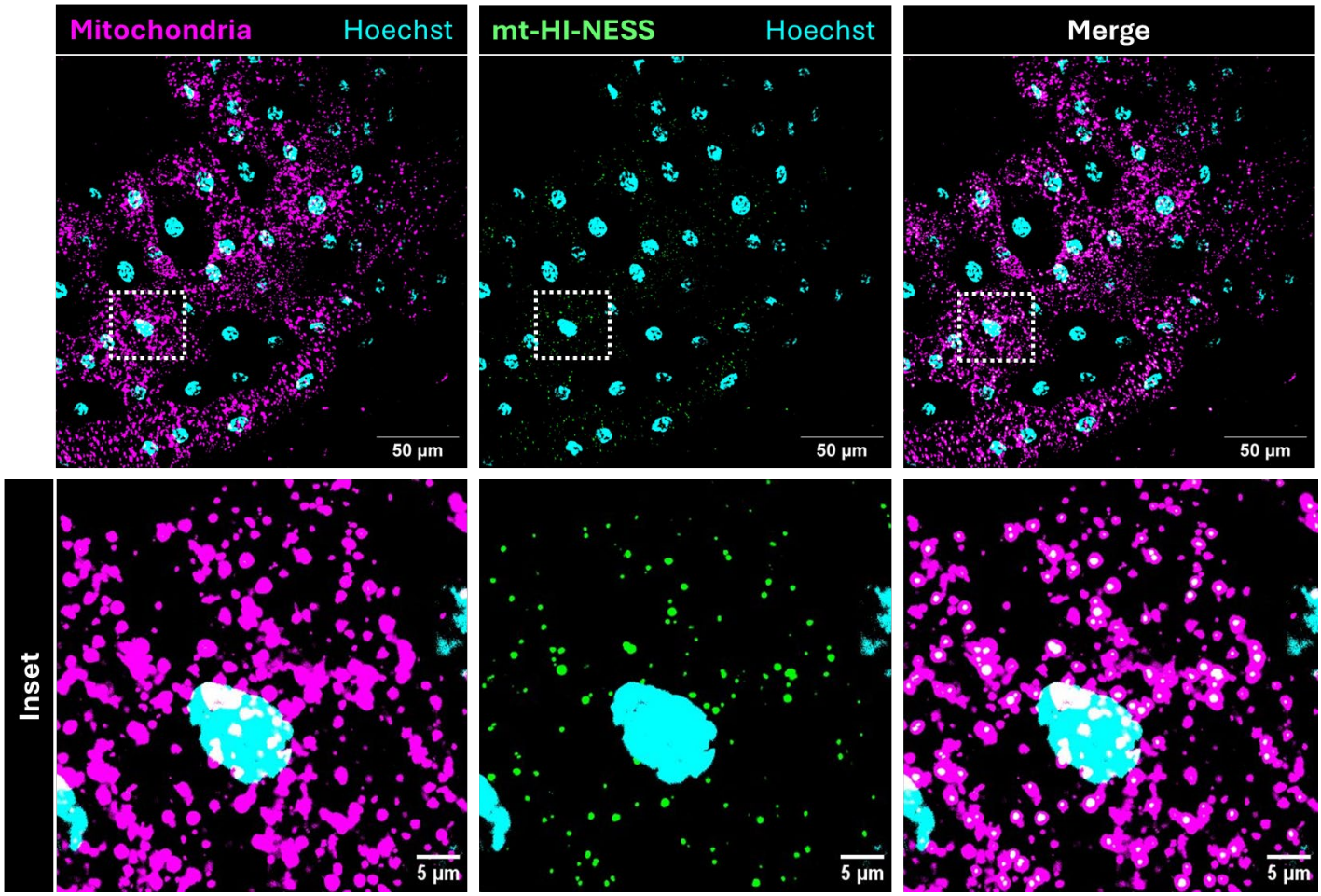

Figure 11: mt-Kaede-HI-NESS in *D. melanogaster* larval fat body. Representative confocal images of the larval fat body tissue from dau-Gal4 crossed to UAS- Kaede mt-HI-NESS. The Kaede mt-HI-NESS (green) is localized within the mitochondrial network (magenta).